Sidelobe Suppression for Multicarrier Signals via Structured Spectral Precoding

Khawar Hussain, *Member, IEEE*, Roberto López-Valcarce, *Senior Member, IEEE*, Francesc Rey, *Member, IEEE*, Josep Sala-Alvarez, *Senior Member, IEEE*, and Javier Villares, *Senior Member, IEEE*

Abstract— **Reducing the large sidelobes of multicarrier signals is crucial to prevent adjacent channel interference. Spectral precoding is an effective approach toward this goal, at the expense of throughput loss due to precoder redundancy; thus, it is of interest to explore alternative precoder designs with improved performance at lower redundancies. We present a novel precoder which minimizes radiated power within a user-selectable frequency region. The structure of the precoding matrix is chosen to allow efficient mitigation of in-band distortion at the receiver by means of iterative and successive interference cancellation, while completely avoiding distortion to protected and pilot subcarriers. By exploiting the low-rank properties of constituent blocks, computational complexity can be significantly reduced with little impact on sidelobe reduction. Simulation results show the benefits of the proposed design, which is particularly effective in redundancy-limited settings targeting high spectral efficiency.**

Index Terms— **Orthogonal frequency division multiplexing (OFDM), spectrum shaping, spectral precoding, out-of-band radiation.**

I. INTRODUCTION

ORTHOGONAL frequency division multiplexing (OFDM) has been adopted as the main signaling format in many wireless communications standards, including 5G New Radio [1] and IEEE 802.11ax (Wi-Fi 6) [2], due to its inherent advantages: it is spectrally efficient, provides robustness against channel dispersion, and is well-matched to multiple input-multiple output (MIMO) operation. Despite these advantages, the power spectral density (PSD) of OFDM signals suffers from large sidelobes, causing high out-of-band radiation (OBR) which results in significant levels of adjacent channel interference. Inserting guard bands by turning off subcarriers is a simple but very inefficient means to address this problem due to the slow decay of sidelobes. Signal filtering [3] and windowing (pulse shaping) [4], [5], [6], [7] are also straightforward, but they reduce the effective length of the cyclic prefix (CP), whereas multiple-choice sequence techniques [8], [9] require the transmission of side information with each symbol, increasing system overhead. Data-dependent techniques have also been proposed, including constellation expansion [10], subcarrier weighting [11], [12], and phase adjustment [13]; they suffer from high online complexity, since they require solving an optimization problem for each OFDM symbol.

Spectral precoding, by which the active subcarriers are modulated by a suitable function of the information symbols, is another approach to reduce OBR [14], [15], [16], [17], [18], [19], [20], [21], [22]. Since it generally introduces in-band distortion, some appropriate decoding may be required at the receiver to mitigate symbol error rate (SER) degradation. Active interference cancellation (AIC) [23], [24], [25], [26], [27], [28], [29], [30] constitutes an exception, as a particular case of spectral precoding in which data symbols are directly mapped to their subcarriers, whereas a few additional cancellation subcarriers, computed as a linear combination of data symbols, are reserved and used for OBR reduction. Although this process is distortionless and hence transparent to the receiver, which merely discards cancellation subcarriers, its effectiveness is limited. In contrast, orthogonal precoders [31], [32], [33], [34] use a precoding matrix with orthonormal columns which does introduce in-band distortion, although its effect can be readily corrected at the receiver without noise enhancement due to the orthonormality property of the precoding matrix. Orthogonal precoders significantly outperform AIC schemes in terms of OBR reduction, but at the price of increased computational complexity at both transmitter and receiver.

With spectral precoding, the difference between the total number of modulated subcarriers and the number of information symbols per block can be thought of as the redundancy of the precoder (e.g., the number of cancellation subcarriers in AIC). Increasing this redundancy results in more degrees of freedom available for OBR reduction, but with the corresponding penalty in spectral efficiency since fewer data symbols per block can be transmitted. At the other extreme, neither

AIC nor orthogonal precoding can provide any OBR reduction with zero redundancy. Thus, it is of interest to seek new low-redundancy precoder designs achieving sufficient sidelobe suppression, possibly at the cost of additional computational complexity, either at the transmitter in order to implement the precoding operation, or at the receiver to compensate in-band distortion [15], [16], [17], [18], [19], [20], [21]. The designs from [19] and [20] provide a step in this direction: the amount of in-band distortion introduced by the precoder can be controlled at the design step, and mitigated at the receiver by means of iterative decoding, as originally proposed in [15]. Larger distortion levels improve OBR performance, but also impose a larger number of iterations at the decoder side.

Motivated by the above considerations, we propose a novel spectral precoder design providing additional flexibility in the tradeoff between OBR reduction and complexity. In particular, and building upon our preliminary work in [20], we combine a precoding block with distortion control on a per-subcarrier basis with a strictly lower triangular band (SLTB) block, whose joint optimization results in improved sidelobe suppression. Moreover, the SLTB structure allows to apply *successive interference cancellation* (SIC) at the receiver, which effectively limits further SER degradation. Following [19], [20], [28], and [33], the proposed design aims to directly minimize OBR over a selectable frequency range. The obtained precoding matrices can be computed offline; in addition, some of these matrices have (approximately) low rank, a property which can be exploited to further reduce online computational cost.

The main contributions of the paper are summarized next:

1) A new structure is proposed for the spectral precoding matrix. Active subcarriers are partitioned into data and cancellation subcarriers, as in AIC, but in-band distortion is allowed in order to improve OBR performance. To counteract its effect, an iterative SIC decoding scheme at the receiver is put forward, which motivates the introduction of a lower triangular block at the precoder side.

2) This lower triangular block is combined with an unstructured low-distortion block for further improvement. Appropriate constraints on in-band distortion facilitate the task of the iterative decoder to avoid error propagation and SER degradation. The proposed structure allows for (but does not require) the inclusion of protected subcarriers, e.g., pilots, which remain free of in-band distortion.

3) Based on this structure, the precoder coefficients are computed in order to minimize OBR, defined as the integral of the weighted PSD over a selectable frequency range. Although the resulting problem is convex, the number of variables and constraints is large, so we propose an alternative low-complexity scheme to iteratively seek a suboptimal solution.

4) We provide numerical examples to validate our design. As it turns out, some of the blocks comprising the precoder can be well approximated by low-rank matrices; similarly, the triangular block of the precoder can be well approximated by a band matrix. These facts result in significant savings in online computational complexity.

The rest of the paper is organized as follows. The signal model is given in Sec. II, and the proposed precoder structure is presented in Sec. III. The optimization problem to obtain the precoder matrices is discussed in Sec. IV, and online complexity is analyzed in Sec. V. Numerical results are provided in Sec. VI, and Sec. VII concludes the paper.

Notation: Vectors and matrices are respectively denoted by boldface lowercase and boldface uppercase symbols. $||\boldsymbol{A}||_F$, $\boldsymbol{A}^T$ and $\boldsymbol{A}^H$ respectively denote the Frobenius norm, the transpose, and the conjugate transpose of $\boldsymbol{A}$. The $n \times n$ identity matrix is denoted as $\boldsymbol{I}_n$, and its i-th column is denoted by $\boldsymbol{e}_i$. The Euclidean norm of a vector $\boldsymbol{v}$ and the trace of a square matrix $\boldsymbol{A}$ are respectively denoted as $||\boldsymbol{v}||$ and $\operatorname{tr} \boldsymbol{A}$. The Kronecker delta is denoted as $\delta[m]$, and $\mathbb{E}\{\cdot\}$ is the expectation operator. Blank blocks in block-partitioned matrices correspond to all-zero blocks.

II. PROBLEM STATEMENT

A. Signal Model

Consider a CP-OFDM signal generated with an IFFT of size N and cyclic prefix size of N_{cp} samples. Let $\mathcal{K} = \{k_1, k_2, \ldots, k_K\}$ denote the set of indices of the $K \leq N$ active subcarriers, and let $x_k[m]$ be the data modulated on the k-th subcarrier in the m-th OFDM symbol. The baseband samples of the multicarrier signal are then given by

$$s[n] = \sum_{m=-\infty}^{\infty} \sum_{k \in \mathcal{K}} x_k[m] h_{\mathrm{P}}[n-mL] \mathrm{e}^{\jmath \frac{2\pi}{N} k(n-mL)}, \quad (1)$$

where $L = N + N_{\mathrm{cp}}$ is the symbol length in samples, and the shaping pulse $h_{\mathrm{P}}[n]$ equals 1 for $n = 0, 1, \ldots, L-1$ and zero elsewhere. The (baseband) continuous-time multicarrier signal is obtained as the output of a digital-to-analog converter (DAC) with sampling frequency $f_s = \frac{1}{T_s}$ with input $s[n]$:

$$s(t) = \sum_{n=-\infty}^{\infty} s[n] h_{\mathrm{I}}(t - nT_s), \quad (2)$$

where $h_{\mathrm{I}}(t)$ is the impulse response of the interpolation filter in the DAC. The subcarrier spacing, in Hz, is then given by $\Delta_f = \frac{1}{N T_s}$.

The allocation of the K active subcarriers is based on four subcarrier types as follows:

- K_{u} subcarriers are dedicated to sending *unprotected data,* i.e., data that may have been altered by the precoding operation. The unprotected data in the m-th symbol are collected in the vector $\boldsymbol{d}_{\mathrm{u}}[m] \in \mathbb{C}^{K_{\mathrm{u}}}$. We define $\boldsymbol{S} \in \mathbb{C}^{N \times K_{\mathrm{u}}}$ as the matrix comprising the K_{u} columns of $\boldsymbol{I}_N$ whose indices correspond to the location of the unprotected data subcarriers.

- K_{p} subcarriers are dedicated to sending *protected data,* i.e., data that should not be distorted by the precoding operation; these are collected in $\boldsymbol{d}_{\mathrm{p}}[m] \in \mathbb{C}^{K_{\mathrm{p}}}$. Protecting data may be necessary in the presence of legacy users which remain oblivious to the precoding operation at the transmitter, or to send side information about the precoder itself [35]. We define $\boldsymbol{R}_{\mathrm{p}} \in \mathbb{C}^{N \times K_{\mathrm{p}}}$ as the matrix comprising the K_{p} columns of $\boldsymbol{I}_N$ whose indices correspond to the location of the protected data subcarriers.

- K_t subcarriers are dedicated to sending *training data* (pilots), which should not be distorted by the precoding operation either [36]. Pilots are collected in $d_\mathrm{t}[m] \in \mathbb{C}^{K_\mathrm{t}}$, and are used for channel estimation and synchronization. Note that $d_\mathrm{t}[m]$ is known at the receiver, whereas $d_\mathrm{u}[m]$, $d_\mathrm{p}[m]$ are not. We define $R_\mathrm{t} \in \mathbb{C}^{N \times K_\mathrm{t}}$ as the matrix comprising the K_t columns of I_N whose indices correspond to the location of the pilot subcarriers.
- K_c subcarriers are reserved for OBR reduction. We define $T \in \mathbb{C}^{N \times K_\mathrm{c}}$ as the matrix comprising the K_c columns of I_N whose indices correspond to the location of these *cancellation subcarriers*.

Thus, one has $K = K_\mathrm{u} + K_\mathrm{p} + K_\mathrm{t} + K_\mathrm{c}$. Note that the allocation matrices S, R_p, R_t, T are all semi-unitary and pairwise orthogonal.

The vector $x[m] = \begin{bmatrix} x_0[m] & x_1[m] & \cdots & x_{N-1}[m] \end{bmatrix}^T \in \mathbb{C}^N$ modulating the subcarriers in the m-th symbol is obtained by linearly precoding the data and the pilots by means of the precoding matrix $G \in \mathbb{C}^{N \times (K_\mathrm{u} + K_\mathrm{p} + K_\mathrm{t})}$. Specifically, letting

$$d[m] \triangleq [\, d_\mathrm{u}^T[m] \quad d_\mathrm{p}^T[m] \quad d_\mathrm{t}^T[m]\,]^T \in \mathbb{C}^{K_\mathrm{u}+K_\mathrm{p}+K_\mathrm{t}}, \quad (3)$$

$$R \triangleq [\, 0_{N \times K_\mathrm{u}} \quad R_\mathrm{p} \quad R_\mathrm{t}\,] \in \mathbb{C}^{N \times (K_\mathrm{u}+K_\mathrm{p}+K_\mathrm{t})}, \quad (4)$$

one has

$$x[m] = (SP + TQ + R)d[m] = Gd[m], \quad (5)$$

where $P \in \mathbb{C}^{K_\mathrm{u} \times (K_\mathrm{u}+K_\mathrm{p}+K_\mathrm{t})}$ and $Q \in \mathbb{C}^{K_\mathrm{c} \times (K_\mathrm{u}+K_\mathrm{p}+K_\mathrm{t})}$ are parameters to be designed. We assume that the subcarrier allocation, defined by the choice of S, T, R_p and R_t, is given. Note that the protected and training data are directly mapped to the corresponding entries of $x[m]$ without distortion: this is readily seen from the fact that $R_\mathrm{p}^H x[m] = [\, 0_{N \times K_\mathrm{u}} \; I_{K_\mathrm{p}} \; 0_{N \times K_\mathrm{t}}\,]d[m] = d_\mathrm{p}[m]$, and $R_\mathrm{t}^H x[m] = [\, 0_{N \times (K_\mathrm{u}+K_\mathrm{p})} \; I_{K_\mathrm{t}}\,]d[m] = d_\mathrm{t}[m]$. Also note that the $N - K$ entries of $x[m]$ with indices not in $\mathcal{K}$ are zero, as they correspond to unmodulated subcarriers.

It is assumed that the sequence $d_\mathrm{t}[m]$ modulated on pilot subcarriers is chosen as pseudo-random with sufficiently long repetition period, in order to avoid undesirable line components in the power spectrum. Thus, $d_\mathrm{t}[m]$ statistically behaves as a truly random sequence approximately, and will be regarded as such. In particular, we assume that $d[m]$ is zero-mean with covariance $\mathbb{E}\{d[m]d^H[m']\} = \delta[m - m']C$, where C is positive definite diagonal, given by

$$C = \begin{bmatrix} I_{K_\mathrm{u}} & \\ & C_\mathrm{pt} \end{bmatrix}, \qquad C_\mathrm{pt} = \begin{bmatrix} C_\mathrm{p} & \\ & C_\mathrm{t} \end{bmatrix}, \quad (6)$$

with $C_\mathrm{p} = \mathrm{diag}\{\, \gamma_{\mathrm{p},1}^2 \; \gamma_{\mathrm{p},2}^2 \cdots \gamma_{\mathrm{p},K_\mathrm{p}}^2 \,\}$ and $C_\mathrm{t} = \mathrm{diag}\{\, \gamma_{\mathrm{t},1}^2 \; \gamma_{\mathrm{t},2}^2 \cdots \gamma_{\mathrm{t},K_\mathrm{t}}^2 \,\}$. Thus, unprotected data have unit variance, whereas the k-th entries of the protected and training data vectors $d_\mathrm{p}[m]$, $d_\mathrm{t}[m]$ have variances $\gamma_{\mathrm{p},k}^2$ and $\gamma_{\mathrm{t},k}^2$, respectively. We allow for $C_\mathrm{pt} \neq I$, since it may be desirable to allocate extra power to protected data and pilots. Hence, $x[m]$ is zero-mean with covariance $\mathbb{E}\{x[m]x^H[m']\} = \delta[m - m']GCG^H$. From this point onwards, we drop the dependence of the vectors $x[m]$, $d[m]$, etc., on the symbol index m, and write simply x, d, etc., unless otherwise specified.

The precoding operation will distort the unprotected data subcarriers whenever $P \neq J$ where

$$J \triangleq [\, I_{K_\mathrm{u}} \quad 0_{K_\mathrm{u} \times (K_\mathrm{p}+K_\mathrm{t})}\,], \quad (7)$$

since in that case $S^H x \neq d_\mathrm{u}$. In general, this in-band distortion will degrade the symbol error rate, unless appropriate measures are taken; typically, these include the application of some decoding algorithm at the receiver exploiting the knowledge of the precoding matrix G and possibly the finite alphabet property of the entries of d.

Note that unprecoded transmission with null subcarriers corresponds to the case $P = J$ and $Q = 0$, i.e., the data subcarriers are undistorted and the cancellation subcarriers are all set to zero. The case $P = J$ with Q optimized to yield low OBR corresponds to AIC; this approach completely avoids data distortion and is transparent to the receiver, which simply discards the cancellation subcarriers. We pursue a more general approach in which both P and Q are optimized, under appropriate constraints.

B. Power Spectral Density

Let $H_\mathrm{P}(\mathrm{e}^{j\omega}) = \sum_n h_\mathrm{P}[n]\mathrm{e}^{-j\omega n}$ and $H_\mathrm{I}(f) = \int_{-\infty}^{\infty} h_\mathrm{I}(t)\mathrm{e}^{-j2\pi ft}\mathrm{d}t$ be the Fourier Transforms of the shaping pulse and DAC interpolation filter, respectively. Also denote

$$\phi_0(f) \triangleq H_\mathrm{P}^*(\mathrm{e}^{j2\pi fT_s}) = \frac{\sin(\pi fT_sL)}{\sin(\pi fT_s)}\mathrm{e}^{j\pi fT_s(L-1)}, \quad (8)$$

$$\phi_k(f) \triangleq \phi_0(f - k\Delta_f), \quad (9)$$

$$\phi(f) \triangleq \begin{bmatrix} \phi_0(f) & \phi_1(f) & \cdots & \phi_{N-1}(f) \end{bmatrix}^T. \quad (10)$$

As shown in [37], the CP-OFDM signal $s(t)$ in (2) is cyclostationary with period LT_s, and with PSD given by

$$S_s(f) = \frac{|H_\mathrm{I}(f)|^2}{LT_s} \cdot \phi^H(f)GCG^H\phi(f) \quad (11)$$

$$= \mathrm{tr}\{G^H\Phi(f)GC\}, \quad (12)$$

where $\Phi(f) \triangleq \frac{|H_\mathrm{I}(f)|^2}{LT_s}\phi(f)\phi^H(f)$ is Hermitian with rank 1.

Given a weight function $W(f) \in [0, 1]\ \forall f$, the corresponding weighted power is given by

$$\mathcal{P}_\mathrm{W} = \int_{-\infty}^{\infty} W(f)S_s(f)\mathrm{d}f = \mathrm{tr}\{G^HA_\mathrm{W}GC\}, \quad (13)$$

where we have introduced the positive (semi-)definite matrix

$$A_\mathrm{W} \triangleq \int_{-\infty}^{\infty} W(f)\Phi(f)\mathrm{d}f \quad \in \quad \mathbb{C}^{N \times N}. \quad (14)$$

To quantify OBR, $W(f)$ can be selected to emphasize certain frequency regions over others; in the simplest case, if $\mathcal{B} \subset \mathbb{R}$ is the set of frequencies over which OBR is to be minimized, one can take $W(f) = 1$ for $f \in \mathcal{B}$ and zero otherwise.

Our goal is to minimize $\mathcal{P}_\mathrm{W}$, given in (13), with respect to P and Q, and subject to appropriate constraints on the total transmit power as well as on the distortion introduced on the data subcarriers, which has a direct impact on decoding complexity at the receiver.

III. PRECODER STRUCTURE

The structure of the precoder impacts both sidelobe suppression capability and in-band distortion. The latter may lead to SER degradation, depending on the decoding strategy applied at the receiver. In this section we present a decoding scheme which, although suboptimal, has low complexity and suggests a suitable structure for the precoder matrix.

At the receiver end, after time and frequency synchronization, the CP is removed and an N-point FFT is applied. From these N samples, those corresponding to the K_c cancellation subcarriers are discarded. Of the remaining ones, the subset of pilot subcarriers can be used for channel estimation and synchronization, since its elements d_t are known and have not been distorted by the precoding operation. After applying frequency-domain equalization, the vectors $r_p \in \mathbb{C}^{K_p}$ and $r_u \in \mathbb{C}^{K_u}$ of protected and unprotected data subcarriers, respectively, are available, and the data vectors d_p, d_u must be recovered from them. Partition P as

$$P = \left[\underbrace{P_u}_{K_u} \quad \underbrace{P_p}_{K_p} \quad \underbrace{P_t}_{K_t} \right], \tag{15}$$

so that $Pd = P_u d_u + P_p d_p + P_t d_t$. For convenience, we also define

$$P_{pt} = \begin{bmatrix} P_p & P_t \end{bmatrix}, \qquad R_{pt} = \begin{bmatrix} R_p & R_t \end{bmatrix}. \tag{16}$$

Then, assuming perfect channel estimation and zero-forcing equalization, one has

$$r_p = d_p + w_p, \tag{17}$$

$$r_u = Pd + w_u$$
$$= P_u d_u + P_p d_p + P_t d_t + w_u, \tag{18}$$

where w_p, w_u are the corresponding noise vectors.

Let $\mathrm{DEC}\{\cdot\}$ be an entrywise operator returning for each entry its closest point in the constellation. Noting from (17) that the protected data symbols can be readily estimated as $\hat{d}_p = \mathrm{DEC}\{r_p\}$, we can substract the effect of the protected and training data from (18) to obtain

$$\tilde{r}_u = r_u - P_p \hat{d}_p - P_t d_t$$
$$\approx P_u d_u + w_u, \tag{19}$$

where it was assumed that $\hat{d}_p \approx d_p$. The receiver needs to recover d_u given $\tilde{r}_u$ in (19); to this end, the structure of the precoding matrix P_u has to be conducive to efficient decoding. Thus, we propose to constrain P_u to be of the form

$$P_u = \Pi(I_{K_u} + \Theta + \Delta), \tag{20}$$

with $\Pi, \Theta, \Delta \in \mathbb{C}^{K_u \times K_u}$ such that:
- Π is a permutation matrix;
- Θ is a strictly lower triangular band matrix [38, Sec. 1.2.1] with bandwidth $b \leq K_u - 1$, i.e., $\Theta_{k\ell} = 0$ if $\ell \geq k$ or $\ell < k - b$;
- Δ is a full matrix with small elements (as described below).

The above structure is motivated by the following iterative decoding procedure, which exploits the finite-alphabet property of data. Let I_{max} be the maximum number of iterations,

and initialize $\hat{d}_u^{(0)} = \mathbb{E}\{d_u\} = 0$. Then, for $i = 1, 2, \ldots, I_{max}$, we first compute the intermediate variable

$$s^{(i)} = \Pi^H \tilde{r}_u - \Delta \hat{d}_u^{(i-1)}, \tag{21}$$

and then, since Θ is strictly lower triangular, apply SIC to obtain the next estimate $\hat{d}_u^{(i)}$ as

$$\hat{d}_{u,1}^{(i)} = \mathrm{DEC}\left\{ s_1^{(i)} \right\},$$

$$\hat{d}_{u,2}^{(i)} = \mathrm{DEC}\left\{ s_2^{(i)} - \Theta_{21} \hat{d}_{u,1}^{(i)} \right\},$$

$$\vdots$$

$$\hat{d}_{u,K_u}^{(i)} = \mathrm{DEC}\left\{ s_{K_u}^{(i)} - \sum_{\ell=1}^{K_u - 1} \Theta_{K_u \ell} \hat{d}_{u,\ell}^{(i)} \right\}. \tag{22}$$

The choice of permutation Π sets the decoding order in the SIC process (21)-(22), and is assumed fixed. Note that, by the band property of Θ, products $\Theta_{k\ell} \hat{d}_{u,\ell}^{(i)}$ are zero for $\ell < k - b$, and need not be computed in (22). By selecting b, complexity can be traded off against OBR reduction performance: larger values of b result in more degrees of freedom for Θ, but also increase the number of complex products required in (22). We denote the set of strictly lower triangular $K_u \times K_u$ band matrices with bandwidth b by $\mathbb{L}_b^{K_u}$.

The effect of the *distortion matrix* Δ is substracted in step (21) based on the estimates from the previous iteration; thus, in order to limit error propagation, the size of the elements of Δ should not be too large, as discussed in Sec. IV.

IV. PRECODER DESIGN

To avoid unacceptable SER degradation at the receiver when the decoding scheme of Sec. III is adopted, some constraint must be placed on the size of the distortion matrix Δ. To this end, note that the normalized inter-carrier interference (ICI) power in the k-th unprotected subcarrier due to this distortion matrix is given by the squared norm of the k-th row of Δ:

$$\frac{\mathbb{E}\{|e_k^H \Delta d_u|^2\}}{\mathbb{E}\{|e_k^H d_u|^2\}} = \|\Delta^H e_k\|^2. \tag{23}$$

Then, it is reasonable to constrain the normalized ICI on a per-subcarrier basis: we set a maximum normalized ICI of $\epsilon_k \ll 1$ for the k-th unprotected data subcarrier.

Another issue that needs to be considered is the potential generation of undesirable spectral peaks in the signal passband. This effect is well known for AIC [25], [39], and results from the optimal precoder giving too much gain to the cancellation subcarriers. Hence, to avoid spectral overshoot in our design, we introduce regularization terms to the cost function $\mathcal{P}_W$ in (13), penalizing large values of the power of the precoded vector components due to the precoding matrices P_{pt}, Q and Θ. Specifically, letting $d_{pt} = [d_p^H \ d_t^H]^H$, these power values are computed as follows:

$$\mathbb{E}\{\|SP_{pt} d_{pt}\|^2\} = \mathrm{tr}\{P_{pt} C_{pt} P_{pt}^H\} = \|P_{pt} C_{pt}^{1/2}\|_F^2, \tag{24}$$

$$\mathbb{E}\{\|TQd\|^2\} = \mathrm{tr}\{QCQ^H\} = \|QC^{1/2}\|_F^2, \tag{25}$$

$$\mathbb{E}\{\|S\Pi\Theta d_u\|^2\} = \mathrm{tr}\{\Theta\Theta^H\} = \|\Theta\|_F^2. \tag{26}$$

Thus, the following problem is obtained:

$$
\min_{\boldsymbol{P}_{\text{pt}}, \boldsymbol{Q}, \boldsymbol{\Delta}, \boldsymbol{\Theta}} \operatorname{tr}\{\boldsymbol{G}^H \boldsymbol{A}_{\text{W}} \boldsymbol{G} \boldsymbol{C}\} + \alpha \|\boldsymbol{P}_{\text{pt}} \boldsymbol{C}_{\text{pt}}^{1/2}\|_F^2
$$
$$
+ \beta \|\boldsymbol{Q}\boldsymbol{C}^{1/2}\|_F^2 + \gamma \|\boldsymbol{\Theta}\|_F^2
$$
$$
\text{s. to} \begin{cases} \boldsymbol{G} = \boldsymbol{S}[\,\boldsymbol{\Pi}(\boldsymbol{I} + \boldsymbol{\Theta} + \boldsymbol{\Delta}) \quad \boldsymbol{P}_{\text{pt}}\,] + \boldsymbol{T}\boldsymbol{Q} + \boldsymbol{R}, \\ \boldsymbol{\Theta} \in \mathbb{L}_b^{K_{\text{u}}}, \\ \epsilon_k \geq \|\boldsymbol{\Delta}^H \boldsymbol{e}_k\|^2, \quad k = 1, \dots, K_{\text{u}}, \end{cases}
$$
$$(27)$$

where $\alpha, \beta, \gamma \geq 0$ are regularization parameters. Their values should be chosen sufficiently large to effectively limit in-band spectral peaks, but not so large as to result in excessive performance loss in terms of OBR. Note that it is not necessary to introduce a regularization term for $\boldsymbol{\Delta}$, as its Frobenius norm is already effectively limited by the per-subcarrier normalized ICI constraints: $\|\boldsymbol{\Delta}\|_F^2 = \sum_{k=1}^{K_{\text{u}}} \|\boldsymbol{\Delta}^H \boldsymbol{e}_k\|^2 \leq \sum_{k=1}^{K_{\text{u}}} \epsilon_k$.

The objective and the K_{u} inequality constraints in (27) are convex quadratic, whereas the remaining constraints are linear. Hence, problem (27) is convex, and it could be tackled with any suitable convex solver. However, this approach quickly becomes impractical as the number of subcarriers increases: the large number of optimization variables and constraints would result in very high computational complexity. This is of particular relevance in dynamic spectrum access (DSA) systems which must reconfigure their transmission parameters as spectrum availability changes over time, so that precoding matrices may have to be frequently recomputed. Due to this, we seek alternative reduced-complexity approaches to approximately solving (27). In particular, we propose to cyclically minimize the objective w.r.t. each of $\{\boldsymbol{P}_{\text{pt}}, \boldsymbol{Q}\}$, $\boldsymbol{\Delta}$, and $\boldsymbol{\Theta}$ while keeping the remaining variables fixed, as follows. Initialize $\boldsymbol{\Delta}_0 = \boldsymbol{0}$ and $\boldsymbol{\Theta}_0 = \boldsymbol{0}$, and then for $j \geq 1$ do:

$$
\{\boldsymbol{P}_{\text{pt},j}, \boldsymbol{Q}_j\} = \arg \min_{\boldsymbol{P}_{\text{pt}}, \boldsymbol{Q}} \mathcal{P}_{\text{W}}(\boldsymbol{P}_{\text{pt}}, \boldsymbol{Q}, \boldsymbol{\Delta}_{j-1}, \boldsymbol{\Theta}_{j-1})
$$
$$
+ \alpha \|\boldsymbol{P}_{\text{pt}} \boldsymbol{C}_{\text{pt}}^{1/2}\|_F^2
$$
$$
+ \beta \|\boldsymbol{Q}\boldsymbol{C}^{1/2}\|_F^2, \tag{28}
$$
$$
\boldsymbol{\Delta}_j = \arg \min_{\boldsymbol{\Delta}} \mathcal{P}_{\text{W}}(\boldsymbol{P}_{\text{pt},j}, \boldsymbol{Q}_j, \boldsymbol{\Delta}, \boldsymbol{\Theta}_{j-1})
$$
$$
\text{s. to } \|\boldsymbol{\Delta}^H \boldsymbol{e}_k\|^2 \leq \epsilon_k, \ 1 \leq k \leq K_{\text{u}}, \tag{29}
$$
$$
\boldsymbol{\Theta}_j = \arg \min_{\boldsymbol{\Theta}} \mathcal{P}_{\text{W}}(\boldsymbol{P}_{\text{pt},j}, \boldsymbol{Q}_j, \boldsymbol{\Delta}_j, \boldsymbol{\Theta}) + \gamma \|\boldsymbol{\Theta}\|_F^2
$$
$$
\text{s. to } \quad \boldsymbol{\Theta} \in \mathbb{L}_b^{K_{\text{u}}}. \tag{30}
$$

At each iteration, the tuple $(\boldsymbol{P}_{\text{pt},j}, \boldsymbol{Q}_j, \boldsymbol{\Delta}_j, \boldsymbol{\Theta}_j)$ is feasible for problem (27); therefore, any convergent point must be feasible, since the feasible set is closed. In addition, the regularized cost function in (27) is decreased (or at most, does not increase) at each of the steps (28)-(30); since this cost function is nonnegative, the sequence of its values necessarily converges.

Each of the three subproblems (28)-(30) is addressed in turn in the following subsections.

A. Optimization of $\{\boldsymbol{P}_{\text{pt}}, \boldsymbol{Q}\}$

For convenience, let us partition $\boldsymbol{Q} = \begin{bmatrix} \boldsymbol{Q}_{\text{u}} & \boldsymbol{Q}_{\text{pt}} \end{bmatrix}$, where $\boldsymbol{Q}_{\text{u}} \in \mathbb{C}^{K_{\text{c}} \times K_{\text{u}}}$ and $\boldsymbol{Q}_{\text{pt}} \in \mathbb{C}^{K_{\text{c}} \times (K_{\text{p}} + K_{\text{t}})}$.

Let $\boldsymbol{P}_{\text{u},j-1} = \boldsymbol{\Pi}(\boldsymbol{I}_{K_{\text{u}}} + \boldsymbol{\Theta}_{j-1} + \boldsymbol{\Delta}_{j-1})$ be fixed, so that (28) is rewritten as

$$
\min_{\boldsymbol{P}_{\text{pt}}, \boldsymbol{Q}} \mathcal{J} \triangleq \operatorname{tr}\{\boldsymbol{G}^H \boldsymbol{A}_{\text{W}} \boldsymbol{G} \boldsymbol{C}\} + \alpha \operatorname{tr}\{\boldsymbol{P}_{\text{pt}}^H \boldsymbol{P}_{\text{pt}} \boldsymbol{C}_{\text{pt}}\}
$$
$$
+ \beta \operatorname{tr}\{\boldsymbol{Q}^H \boldsymbol{Q} \boldsymbol{C}\}
$$
$$
\text{s. to } \boldsymbol{G} = \boldsymbol{S}[\,\boldsymbol{P}_{\text{u},j-1} \ \boldsymbol{P}_{\text{pt}}\,] + \boldsymbol{T}\boldsymbol{Q} + \boldsymbol{R}. \tag{31}
$$

This is a convex quadratic problem, whose solution can be found in closed form as follows. Let us partition the precoding matrix as $\boldsymbol{G} = [\,\boldsymbol{G}_{\text{u}} \ \boldsymbol{G}_{\text{pt}}\,]$, where $\boldsymbol{G}_{\text{u}} = \boldsymbol{S}\boldsymbol{P}_{\text{u},j-1} + \boldsymbol{T}\boldsymbol{Q}_{\text{u}}$ and $\boldsymbol{G}_{\text{pt}} = \boldsymbol{S}\boldsymbol{P}_{\text{pt}} + \boldsymbol{T}\boldsymbol{Q}_{\text{pt}} + \boldsymbol{R}_{\text{pt}}$. In view of (6), the first and third terms of the cost $\mathcal{J}$ in (31) can be written respectively as

$$
\operatorname{tr}\{\boldsymbol{G}^H \boldsymbol{A}_{\text{W}} \boldsymbol{G} \boldsymbol{C}\} = \operatorname{tr}\{\boldsymbol{G}_{\text{u}}^H \boldsymbol{A}_{\text{W}} \boldsymbol{G}_{\text{u}}\}
$$
$$
+ \operatorname{tr}\{\boldsymbol{G}_{\text{pt}}^H \boldsymbol{A}_{\text{W}} \boldsymbol{G}_{\text{pt}} \boldsymbol{C}_{\text{pt}}\}, \tag{32}
$$
$$
\beta \operatorname{tr}\{\boldsymbol{Q}^H \boldsymbol{Q} \boldsymbol{C}\} = \beta \operatorname{tr}\{\boldsymbol{Q}_{\text{u}}^H \boldsymbol{Q}_{\text{u}}\}
$$
$$
+ \beta \operatorname{tr}\{\boldsymbol{Q}_{\text{pt}}^H \boldsymbol{Q}_{\text{pt}} \boldsymbol{C}_{\text{pt}}\}. \tag{33}
$$

We recall the following properties of the complex gradient[1]: for constant matrices $\boldsymbol{A}$, $\boldsymbol{B}$, it holds that $\nabla_{\boldsymbol{X}} \operatorname{tr}\{\boldsymbol{X}^H \boldsymbol{A}\} = \boldsymbol{A}$, $\nabla_{\boldsymbol{X}} \operatorname{tr}\{\boldsymbol{A}^H \boldsymbol{X}\} = \boldsymbol{0}$, and $\nabla_{\boldsymbol{X}} \operatorname{tr}\{\boldsymbol{X}^H \boldsymbol{A}\boldsymbol{X}\boldsymbol{B}\} = \boldsymbol{A}\boldsymbol{X}\boldsymbol{B}$. Then one has

$$
\nabla_{\boldsymbol{P}_{\text{pt}}} \mathcal{J} = \boldsymbol{S}^H \boldsymbol{A}_{\text{W}} \boldsymbol{S}\boldsymbol{P}_{\text{pt}} \boldsymbol{C}_{\text{pt}} + \boldsymbol{S}^H \boldsymbol{A}_{\text{W}}(\boldsymbol{T}\boldsymbol{Q}_{\text{pt}} + \boldsymbol{R}_{\text{pt}})
$$
$$
+ \alpha \boldsymbol{P}_{\text{pt}} \boldsymbol{C}_{\text{pt}}, \tag{34}
$$
$$
\nabla_{\boldsymbol{Q}_{\text{pt}}} \mathcal{J} = \boldsymbol{T}^H \boldsymbol{A}_{\text{W}} \boldsymbol{T}\boldsymbol{Q}_{\text{pt}} \boldsymbol{C}_{\text{pt}} + \boldsymbol{T}^H \boldsymbol{A}_{\text{W}}(\boldsymbol{S}\boldsymbol{P}_{\text{pt}} + \boldsymbol{R}_{\text{pt}})
$$
$$
+ \beta \boldsymbol{Q}_{\text{pt}} \boldsymbol{C}_{\text{pt}}, \tag{35}
$$
$$
\nabla_{\boldsymbol{Q}_{\text{u}}} \mathcal{J} = \boldsymbol{T}^H \boldsymbol{A}_{\text{W}} \boldsymbol{T}\boldsymbol{Q}_{\text{u}} + \boldsymbol{T}^H \boldsymbol{A}_{\text{W}} \boldsymbol{S}\boldsymbol{P}_{\text{u},j-1} + \beta \boldsymbol{Q}_{\text{u}}. \tag{36}
$$

Since $\boldsymbol{C}_{\text{pt}}$ is invertible, equating (34)-(36) to zero yields the solution to (31):

$$
\boldsymbol{Q}_{\text{u},j} = -(\boldsymbol{T}^H \boldsymbol{A}_{\text{W}} \boldsymbol{T} + \beta \boldsymbol{I}_{K_{\text{c}}})^{-1} \boldsymbol{T}^H \boldsymbol{A}_{\text{W}} \boldsymbol{S}\boldsymbol{P}_{\text{u},j-1},
$$
$$(37)$$
$$
\begin{bmatrix} \boldsymbol{P}_{\text{pt},j} \\ \boldsymbol{Q}_{\text{pt},j} \end{bmatrix} = -(\boldsymbol{Z}^H \boldsymbol{A}_{\text{W}} \boldsymbol{Z} + \boldsymbol{D})^{-1} \boldsymbol{Z}^H \boldsymbol{A}_{\text{W}} \boldsymbol{R}_{\text{pt}}, \tag{38}
$$

where we have introduced the matrices

$$
\boldsymbol{Z} = \begin{bmatrix} \boldsymbol{S} & \boldsymbol{T} \end{bmatrix}, \qquad \boldsymbol{D} = \begin{bmatrix} \alpha \boldsymbol{I}_{K_{\text{u}}} & \\ & \beta \boldsymbol{I}_{K_{\text{c}}} \end{bmatrix}. \tag{39}
$$

Note that (38) is in fact independent of the iteration index j, so it only has to be computed once.

B. Optimization of $\boldsymbol{\Delta}$

For fixed $\boldsymbol{P}_{\text{pt}} = \boldsymbol{P}_{\text{pt},j}$, $\boldsymbol{Q} = \boldsymbol{Q}_j$ and $\boldsymbol{\Theta} = \boldsymbol{\Theta}_{j-1}$, problem (29) becomes

$$
\min_{\boldsymbol{\Delta}} \operatorname{tr}\{\boldsymbol{G}^H \boldsymbol{A}_{\text{W}} \boldsymbol{G} \boldsymbol{C}\} \tag{40}
$$
$$
\text{s.to} \begin{cases} \epsilon_k \geq \|\boldsymbol{\Delta}^H \boldsymbol{e}_k\|^2, \quad k = 1, \dots, K_{\text{u}}, \\ \boldsymbol{G} = \boldsymbol{S}[\,\boldsymbol{\Pi}(\boldsymbol{I}_{K_{\text{u}}} + \boldsymbol{\Theta}_{j-1} + \boldsymbol{\Delta}) \ \boldsymbol{P}_{\text{pt},j}\,] \\ \quad + \boldsymbol{T}\boldsymbol{Q}_j + \boldsymbol{R}. \end{cases} \tag{41}
$$

The main hurdle towards efficiently solving (40)-(41) is the large number of inequality constraints related to the per-subcarrier normalized ICI power. Noting that each of these

---

[1] Writing the complex-valued matrix $\boldsymbol{X} = [\,\boldsymbol{x}_1 \cdots \boldsymbol{x}_n\,]$ columnwise, the gradient of a scalar, real-valued function f w.r.t. $\boldsymbol{X}$ is defined also columnwise as $\nabla_{\boldsymbol{X}} f = [\nabla_{\boldsymbol{x}_1} f \cdots \nabla_{\boldsymbol{x}_n} f]$, with $\nabla_{\boldsymbol{x}} f = \frac{1}{2}[\nabla_{\text{Re}\,\boldsymbol{x}} f + j \nabla_{\text{Im}\,\boldsymbol{x}} f]$.

constraints involves a single row of $\mathbf{\Delta}$, we propose to sequentially minimize the objective with respect to each of these rows while keeping the remaining $K_\mathrm{u} - 1$ rows fixed. To this end, let $\boldsymbol{\delta}_k = \mathbf{\Delta}^H \boldsymbol{e}_k$, and let $\overline{\mathbf{\Delta}}_k = \mathbf{\Delta} - \boldsymbol{e}_k \boldsymbol{\delta}_k^H$, i.e., $\overline{\mathbf{\Delta}}_k$ is obtained by zeroing out the k-th row of $\mathbf{\Delta}$. With these, let us introduce

$$\overline{\boldsymbol{G}}_{j,k} = \boldsymbol{S} \left[\mathbf{\Pi}(\boldsymbol{I}_{K_\mathrm{u}} + \mathbf{\Theta}_{j-1} + \overline{\mathbf{\Delta}}_k) \ \ \boldsymbol{P}_{\mathrm{pt},j} \right] + \boldsymbol{T}\boldsymbol{Q}_j + \boldsymbol{R}, \tag{42}$$

which does not depend on $\boldsymbol{\delta}_k$. Then the precoder matrix can be written as $\boldsymbol{G} = \overline{\boldsymbol{G}}_{j,k} + \boldsymbol{S}\mathbf{\Pi}\boldsymbol{e}_k \boldsymbol{\delta}_k^H \boldsymbol{J}$, where $\boldsymbol{J}$ was defined in (7). Therefore, the problem of optimizing $\boldsymbol{\delta}_k$ while keeping $\overline{\mathbf{\Delta}}_k$ fixed can be stated as

$$\min_{\boldsymbol{\delta}_k} \operatorname{tr}\{\boldsymbol{G}^H \boldsymbol{A}_\mathrm{W} \boldsymbol{G} \boldsymbol{C}\} \tag{43}$$

$$\text{s.to} \begin{cases} \|\boldsymbol{\delta}_k\|^2 \leq \epsilon_k, \\ \boldsymbol{G} = \overline{\boldsymbol{G}}_{j,k} + \boldsymbol{S}\mathbf{\Pi}\boldsymbol{e}_k \boldsymbol{\delta}_k^H \boldsymbol{J}. \end{cases} \tag{44}$$

This convex quadratic problem with a quadratic inequality constraint is highly structured and can be solved in closed form, as shown in Appendix A. In this way, the rows of $\mathbf{\Delta}$ are optimized in a sequential fashion. The order of the sequence may be cyclic or random, and the number of passes can be either fixed, or variable subject to some stopping criterion. Note that in (44), j denotes the index of the outer iterations corresponding to (28)-(30), whereas k is the index of the inner iterations corresponding to the row updates with j fixed.

C. Optimization of $\mathbf{\Theta}$

For fixed $\boldsymbol{P}_\mathrm{pt} = \boldsymbol{P}_{\mathrm{pt},j}$, $\boldsymbol{Q} = \boldsymbol{Q}_j$ and $\mathbf{\Delta} = \mathbf{\Delta}_j$, problem (30) becomes

$$\min_{\mathbf{\Theta}} \operatorname{tr}\{\boldsymbol{G}^H \boldsymbol{A}_\mathrm{W} \boldsymbol{G} \boldsymbol{C}\} + \gamma \|\mathbf{\Theta}\|_F^2 \tag{45}$$

$$\text{s.to} \begin{cases} \mathbf{\Theta} \in \mathbb{L}_b^{K_\mathrm{u} \times K_\mathrm{u}}, \\ \boldsymbol{G} = \boldsymbol{S} \left[\mathbf{\Pi}(\boldsymbol{I}_{K_\mathrm{u}} + \mathbf{\Theta} + \mathbf{\Delta}_j) \ \ \boldsymbol{P}_{\mathrm{pt},j} \right] \\ + \boldsymbol{T}\boldsymbol{Q}_j + \boldsymbol{R}. \end{cases} \tag{46}$$

Note that the constraint $\mathbf{\Theta} \in \mathbb{L}_b^{K_\mathrm{u} \times K_\mathrm{u}}$ is linear in $\mathbf{\Theta}$. Then the objective in (45) can be written in terms of the nonzero elements of $\mathbf{\Theta}$, resulting in a convex quadratic problem (see Appendix B). The overall procedure for computing the precoder $\boldsymbol{G} = \boldsymbol{S}\boldsymbol{P} + \boldsymbol{T}\boldsymbol{Q} + \boldsymbol{R}$ is summarized in Algorithm 1.

V. COMPLEXITY ANALYSIS

Implementation complexity is a critical factor for any OBR reduction method, both at transmitter and receiver. Our design of precoder matrices can be done offline, as it is data-independent. Regarding online complexity, one has:

- At the transmitter, directly implementing (5) requires $(K_\mathrm{u} + K_\mathrm{c})(K_\mathrm{u} + K_\mathrm{p} + K_\mathrm{t})$ complex multiplications per OFDM symbol (cmults/symb).
- At the receiver end, since $\boldsymbol{d}_\mathrm{t}$ is known, the term $\boldsymbol{P}_\mathrm{t}\boldsymbol{d}_\mathrm{t}$ can be precomputed and stored, so the initial step (19) requires $K_\mathrm{u} K_\mathrm{p}$ cmults. The intermediate step (21) requires K_u^2 cmults/symb per iteration, except for the first iteration which is multiplication-free; whereas the number

---

Algorithm 1 Structured Spectral Precoder Design

1: Input: subcarrier allocation matrices $\{\boldsymbol{S}, \boldsymbol{T}, \boldsymbol{R}\}$, OBR matrix $\boldsymbol{A}_\mathrm{W}$, covariance matrix $\boldsymbol{C}$, permutation matrix $\mathbf{\Pi}$, bandwidth b, normalized ICI constraints $\{\epsilon_k\}_{k=1}^{K_\mathrm{u}}$, regularization factors α, β, γ
2: Initialize $\mathbf{\Delta}_0 \leftarrow \mathbf{0}_{K_\mathrm{u} \times K_\mathrm{u}}$, $\mathbf{\Theta}_0 \leftarrow \mathbf{0}_{K_\mathrm{u} \times K_\mathrm{u}}$, $j = 1$
3: **repeat**
4:     Compute $\boldsymbol{Q}_{\mathrm{u},j}$, $\boldsymbol{Q}_{\mathrm{pt},j}$, $\boldsymbol{P}_{\mathrm{pt},j}$ via (37), (38)
5:     Set $\boldsymbol{Q}_j \leftarrow [\boldsymbol{Q}_{\mathrm{u},j} \ \boldsymbol{Q}_{\mathrm{pt},j}]$ and $\mathbf{\Delta} \leftarrow \mathbf{\Delta}_{j-1}$
6:     **repeat**
7:         pick $k \in \{1, \ldots, K_\mathrm{u}\}$ and set $\overline{\boldsymbol{G}}_{j,k}$ as per (42)
8:         find $\boldsymbol{\delta}_k$ by solving (43)-(44) as per Appendix A
9:         overwrite the k-th column of $\mathbf{\Delta}$ with $\boldsymbol{\delta}_k$
10:     **until** no change in $\mathbf{\Delta}$
11:     set $\mathbf{\Delta}_j \leftarrow \mathbf{\Delta}$
12:     find $\mathbf{\Theta}_j$ by solving (45) as per Appendix B
13:     set $\boldsymbol{P}_j \leftarrow [\mathbf{\Pi}(\boldsymbol{I}_{K_\mathrm{u}} + \mathbf{\Theta}_j + \mathbf{\Delta}_j) \ \boldsymbol{P}_{\mathrm{pt},j}]$
14:     set $j \leftarrow j + 1$
15: **until** no change in $\{\boldsymbol{P}_j, \boldsymbol{Q}_j\}$

---

of cmults/symb in the SIC step (22) is $b(K_\mathrm{u} - b) + \frac{1}{2}b(b-1) \leq bK_\mathrm{u}$ per iteration.[2] Interestingly, as shown in Sec. VI, the matrix $\mathbf{\Delta}$ obtained by the proposed design tends to have many small singular values, which is reasonable since the constraints on normalized ICI prevent $\mathbf{\Delta}$ from being "large". This property motivates the use of a low-rank approximation of $\mathbf{\Delta}$ to reduce implementation complexity. The best choice, in the sense of minimizing the squared Frobenius norm of the approximation error, is given by truncating the singular value decomposition (SVD), as per the Eckart-Young theorem [40]. Thus, if the SVD of $\mathbf{\Delta}$ is truncated to $r_\Delta < K_\mathrm{u}$ principal components, then

$$\mathbf{\Delta} \approx \boldsymbol{L}_\Delta \boldsymbol{M}_\Delta^H, \tag{47}$$

for some $\boldsymbol{L}_\Delta \in \mathbb{C}^{K_\mathrm{u} \times r_\Delta}$ and $\boldsymbol{M}_\Delta \in \mathbb{C}^{K_\mathrm{u} \times r_\Delta}$. Then the transmitter computes (5) as

$$\begin{aligned} \boldsymbol{x} = &\boldsymbol{S}\mathbf{\Pi}(\boldsymbol{d}_\mathrm{u} + \mathbf{\Theta}\boldsymbol{d}_\mathrm{u} + \boldsymbol{L}_\Delta(\boldsymbol{M}_\Delta^H \boldsymbol{d}_\mathrm{u})) \\ & + \boldsymbol{S}(\boldsymbol{P}_\mathrm{p}\boldsymbol{d}_\mathrm{p} + \boldsymbol{P}_\mathrm{t}\boldsymbol{d}_\mathrm{t}) + \boldsymbol{T}\boldsymbol{Q}\boldsymbol{d} + \boldsymbol{R}\boldsymbol{d}, \end{aligned} \tag{48}$$

which, taking into account that the terms involving $\boldsymbol{d}_\mathrm{t}$ can be precomputed and stored, requires $b(K_\mathrm{u} - \frac{1}{2}(b+1)) + 2r_\Delta K_\mathrm{u} + K_\mathrm{u} K_\mathrm{p} + K_\mathrm{c}(K_\mathrm{u} + K_\mathrm{p})$ cmults/symb. Analogously, at the receiver end, the intermediate step (21) can be implemented with $2r_\Delta K_\mathrm{u}$ cmults/symb per iteration. This results in significant savings, because usually it is possible to take $r_\Delta \ll K_\mathrm{u}$ without significantly compromising OBR reduction.

VI. NUMERICAL EXAMPLES

We provide examples of the performance of the proposed design. For reference, we compare the corresponding PSD

---

[2]Note that this figure may be actually lower if one exploits the finite-alphabet nature of past decisions: for instance, with Quadrature Phase-Shift Keying (QPSK) modulation, the terms $\hat{d}_{\mathrm{u},\ell}^{(i)}$ in (22) belong in $\{1+j, 1-j, -1+j, -1-j\}$, so that $\Theta_{k\ell}\hat{d}_{\mathrm{u},\ell}^{(i)}$ can be actually computed with just two real additions; similar considerations apply to the computation of $\mathbf{\Delta}\hat{d}_\mathrm{u}^{(i-1)}$ in (21). Nevertheless, we do not take such potential savings into account when reporting computational loads.
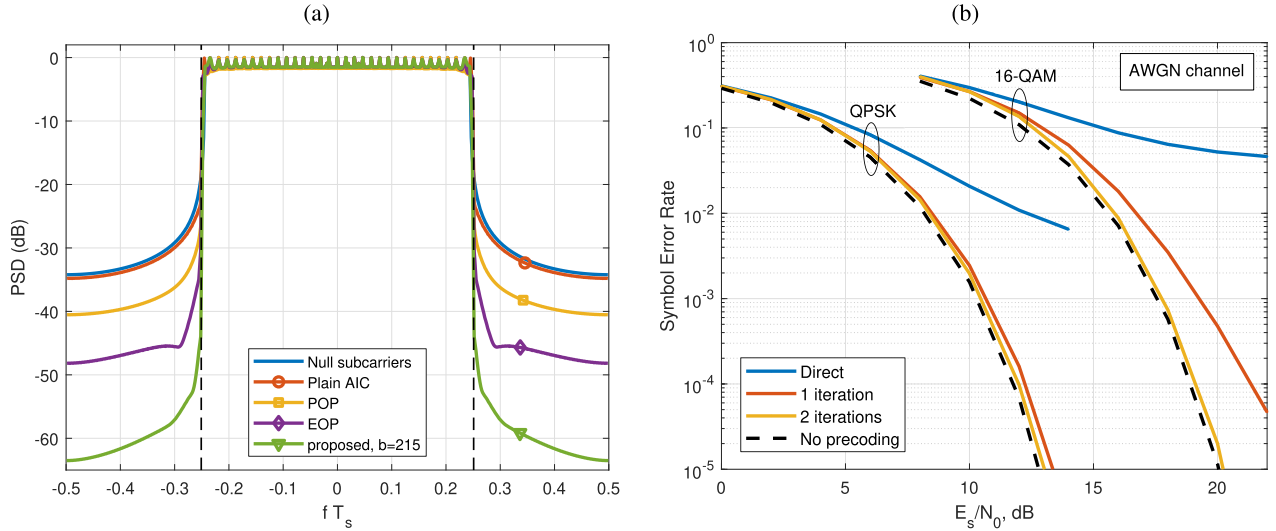
Fig. 1. Scenario 1: $K_c = 6$, $\epsilon = 0.005$, $b = 215$. (a) PSD envelope of different designs. Dashed vertical lines mark the boundary of the OBR region; (b) Symbol error rate with the proposed decoding scheme.

with those of a plain CP-OFDM system with null subcarriers and no precoding ($\boldsymbol{P} = \boldsymbol{J}$ and $\boldsymbol{Q} = \boldsymbol{0}$), the standard AIC design ($\boldsymbol{P} = \boldsymbol{J}$), and two variations of Orthogonal Precoding to accommodate protected and training subcarriers, termed *Plain Orthogonal Precoding* (POP) and *Extended Orthogonal Precoding* (EOP), which are described in Appendix C. In both cases the design criterion is the minimization of the weighted power (13); the structure of EOP is an extension of that proposed in [35], which considered data and pilot subcarriers, to also allow for protected subcarriers not known at the receiver. If all subcarriers are unprotected, POP and EOP reduce to the design from [33].

Assuming an ideal lowpass interpolation filter $H_I(f)$ with cutoff frequency $f_s/2$, three different scenarios are examined for a transmitter with IFFT size $N = 512$ and CP length $N_{cp} = N/16$, which differ in the number and layout of active subcarriers. In all cases, all protected subcarriers have the same power $\gamma_{p,k}^2 = 1.2$, whereas all training subcarriers have power $\gamma_{t,k}^2 = 1.5$. The permutation matrix $\boldsymbol{\Pi} \in \mathbb{C}^{K_u \times K_u}$ is taken as

$$\boldsymbol{\Pi} = \begin{bmatrix} \boldsymbol{e}_{\frac{K_u}{2}} & \boldsymbol{e}_{\frac{K_u}{2}+1} & \boldsymbol{e}_{\frac{K_u}{2}-1} & \boldsymbol{e}_{\frac{K_u}{2}+2} & \cdots & \boldsymbol{e}_1 & \boldsymbol{e}_{K_u} \end{bmatrix}. \tag{49}$$

With this choice, the SIC decoder starts with the innermost subcarrier, and then progresses incrementally towards the band edges alternating between subcarriers below and above the passband center. This decoding order has been found to yield a more uniform distribution of power across subcarriers, resulting in a PSD with reduced in-band spectral peaks. In all designs, the regularization factors are selected by trial and error in order to obtain the best performance in terms of OBR reduction without incurring in spectral overshoot. They are expressed in terms of the product of dimensions of the corresponding matrices, e.g., for α, β, γ in (27) we write $\alpha = \bar{\alpha} K_u(K_p + K_t)$, $\beta = \bar{\beta} K_c(K_u + K_p + K_t)$, $\gamma = \bar{\gamma} K_u^2$, whereas for α' in (65), we write $\alpha' = \bar{\alpha}'(K_u + K_c)(K_p + K_t)$.

A. Scenario 1

We consider a layout with $K = 257$ active subcarriers symmetrically located about the carrier frequency, *i.e.,* $\mathcal{K} = \{-128, \cdots, 0, \cdots, 128\}$. There are $K_p = 4$ protected subcarriers, with indices in $\mathcal{K}_p = \{\pm 10, \pm 20\}$, and $K_t = 31$ training subcarriers, with indices in $\mathcal{K}_t = \{0, \pm 8, \pm 16, \cdots, \pm 112, \pm 120\}$, so $K_u = 222 - K_c$. The OBR region is $\mathcal{B} = \{\frac{f_s}{4} + \frac{\Delta_f}{2} \leq |f| \leq \frac{f_s}{2}\}$, with weight $W(f) = 1$ for $f \in \mathcal{B}$ and 0 elsewhere. The K_c cancellation subcarriers are symmetrically placed at the lower and upper edges of the passband, with indices in $\mathcal{K}_c = \{-128, -127, \cdots, -128 + (\frac{K_c}{2} - 1), 128 - (\frac{K_c}{2} - 1), \ldots, 127, 128\}$. It is assumed that K_c is even, so that K_u is even as well.

Fig. 1(a) shows the PSD obtained in this setting by the different precoder designs, all of them with $K_c = 6$ cancellation subcarriers; thus, the precoder redundancy is $\frac{K_c}{K} = 2.3\%$ (only the PSD envelope is shown for clarity). The extra power allocated to protected and pilot subcarriers makes their locations within the passband clearly noticeable. The AIC precoding design ($\bar{\beta} = 16$) provides little OBR reduction with respect to the reference scheme using $K_c/2$ null subcarriers at each passband edge, whereas the orthogonal designs (POP and EOP, $\bar{\alpha}' = 0$) perform significantly better. For the proposed design, we initially constrain the normalized ICI power to $\epsilon_k = \epsilon = 0.005 \; \forall k$ and $b = K_u - 1 = 215$, so that all the degrees of freedom available in the precoding matrix $\boldsymbol{\Theta}$ are used. The proposed design ($\bar{\alpha} = 0.2$, $\bar{\beta} = 0.3$, $\bar{\gamma} = 0.005$) significantly outperforms the other schemes, providing lower PSD levels in the OBR region. The SER obtained with the decoding scheme described in Sec. III is shown in Fig. 1(b), assuming an additive white Gaussian noise (AWGN) channel. It is seen that directly slicing the vector $\widetilde{\boldsymbol{r}}_u$ in (19) yields poor performance (curve labeld "direct" in the figure), due to intercarrier interference introduced by the precoding matrix $\boldsymbol{P}_u$. The SIC-based decoder effectively counteracts this effect with just two iterations in this case, for both QPSK and 16-QAM modulation.

TABLE I

OBR LOSS INCURRED BY A LOW-RANK APPROXIMATION OF $\boldsymbol{\Delta}$. SCENARIO 1, $N = 512$, $K_{\mathrm{c}} = 6$, $\epsilon = 0.005$, $b = 215$

r_Δ	1	2	3	4	5	6	7	8	9	10
dB	21.1	16.2	15.3	13.7	8.2	5.1	0.9	0.6	0.1	0.05

TABLE II

ONLINE COMPLEXITY (IN CMULTS/SYMB AND AS PERCENTAGE OF IFFT/FFT COMPUTATIONAL COST $\frac{N}{2} \log_2 N$) AT TX AND RX, AND OBR REDUCTION (IN dBr) FOR DIFFERENT DESIGNS. SCENARIO 1, $N = 512$, $K_{\mathrm{c}} = 6$, $\epsilon = 0.005$, $r_\Delta = 7$, TWO DECODING ITERATIONS

	AIC	POP	EOP	$b = 0$	$b = 2$	$b = 4$	$b = 10$	$b = 20$	$b = 50$
TX	1320 (57%)	2628 (114%)	3516 (153%)	5208 (226%)	5637 (245%)	6062 (263%)	7313 (317%)	9318 (404%)	14 733 (639%)
RX	–	2628 (114%)	3516 (153%)	3888 (169%)	4746 (206%)	5596 (243%)	8098 (351%)	12 108 (525%)	22 938 (996%)
dBr	2.3	7.1	14.8	10.9	20.8	23.1	24.1	26.0	28.2

To explore more computationally efficient alternatives, let us introduce two energy compaction metrics applied to the $K_{\mathrm{u}} \times K_{\mathrm{u}}$ matrices $\boldsymbol{\Theta}$ and $\boldsymbol{\Delta}$, respectively. For the strictly lower triangular $\boldsymbol{\Theta}$, we define the energy compaction over subdiagonals as the energy of all coefficients in subdiagonals 1 through k, normalized by the total energy, *i.e.,*

$$D_k(\boldsymbol{\Theta}) = \frac{\sum_{i=1}^{k} \sum_{j=1}^{K_{\mathrm{u}}-1} |\boldsymbol{\Theta}_{i+j,j}|^2}{\|\boldsymbol{\Theta}\|_F^2}, \quad k = 1, 2, \ldots, K_{\mathrm{u}} - 1, \tag{50}$$

whereas for the matrix $\boldsymbol{\Delta}$, we measure the energy compaction over its singular values $\sigma_1(\boldsymbol{\Delta}) \geq \sigma_2(\boldsymbol{\Delta}) \geq \ldots \geq \sigma_{K_{\mathrm{u}}}(\boldsymbol{\Delta})$ as

$$F_k(\boldsymbol{\Delta}) = \frac{\sum_{i=1}^{k} \sigma_i^2(\boldsymbol{\Delta})}{\|\boldsymbol{\Delta}\|_F^2}, \quad k = 1, 2, \ldots, K_{\mathrm{u}}. \tag{51}$$

Note that $D_{K_{\mathrm{u}}-1}(\boldsymbol{\Theta}) = 1$ and $F_{K_{\mathrm{u}}}(\boldsymbol{\Delta}) = 1$ always hold. From Fig. 2, it is seen that the most significant coefficients of $\boldsymbol{\Theta}$ are grouped in the first subdiagonals (for example, the first 60 subdiagonals pack over 90% of the total energy), and that $\boldsymbol{\Delta}$ has a small number of significant singular values. These observations motivate the adoption of a banded structure for $\boldsymbol{\Theta}$ and a low-rank approximation for $\boldsymbol{\Delta}$, in order to reduce computational complexity with a small impact on performance. To check this point, Table I shows the performance loss incurred by replacing $\boldsymbol{\Delta}$ by its best r_Δ-rank approximation: it is seen that as long as $r_\Delta \geq 7$, the loss is below 1 dB.

Next, the precoder was redesigned keeping the normalized ICI power constraint $\epsilon = 0.005$, but with different values of the bandwidth $b \in \{0, 2, 4, 10, 20, 50\}$; the resulting matrix $\boldsymbol{\Delta}$ was replaced by its best rank-7 approximation in all cases with very small performance loss. Fig. 3(a) shows the corresponding PSDs. For $b = 0$ (meaning the triangular component $\boldsymbol{\Theta}$ is absent in the precoder) the proposed design performs better than POP but worse than EOP. However, for $b \geq 2$ the proposed scheme outperforms EOP. The PSD obtained with $b = 50$ is nearly identical to that with $b = 215$.

The convergence of the proposed method in terms of OBR reduction (relative to the OBR achieved with the null subcarriers-based reference scheme) is shown in Fig. 3(b), together with the corresponding values obtained with AIC, POP and EOP. In general, convergence is smooth but takes longer for larger b. For all values of b, the observed SER
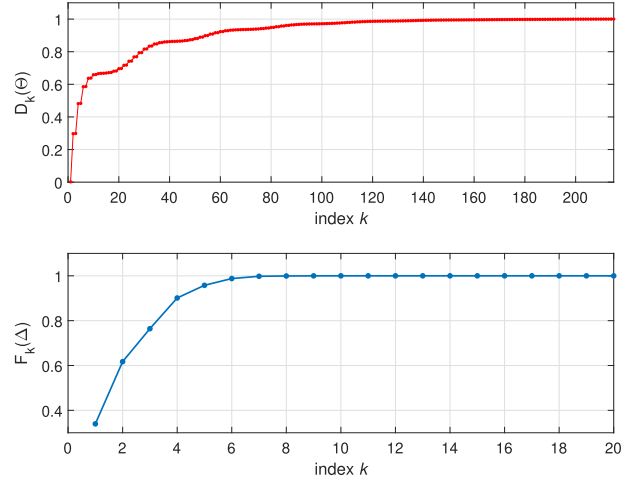
Fig. 2. Scenario 1: $K_{\mathrm{c}} = 6$, $\epsilon = 0.005$, $b = 215$. Energy compaction metrics $D_k(\boldsymbol{\Theta})$ (top) and $F_k(\boldsymbol{\Delta})$ (bottom).

behavior of the decoder in the AWGN channel was similar to that in Fig. 1(b), taking two iterations to converge. Table II lists the online complexity of the different designs in this setting, both at the transmitter and at the receiver, together with the attained OBR reduction. With $b = 50$, OBR is 13.4 dB below that of EOP, at the price of increased complexity (by a factor of 4.2 at the transmitter and 6.5 at the receiver, approximately). The value of b can be further decreased to trade off performance and complexity; for example, with $b = 4$ it is possible to achieve an OBR improvement of 8.3 dB over EOP, at about twice its computational cost.

In the next experiment, still with $K_{\mathrm{c}} = 6$, the bandwidth of $\boldsymbol{\Theta}$ was fixed to $b = 10$, and the value of the normalized ICI power constraint $\epsilon_k = \epsilon$ (common to all unprotected subcarriers) was varied as $\epsilon \in \{0, 0.0025, 0.01, 0.015\}$. Note that $\epsilon = 0$ means that the term $\boldsymbol{\Delta}$ is absent in (20); for $\epsilon > 0$, a low-rank approximation of $\boldsymbol{\Delta}$ was adopted using $r_\Delta = 7$. The resulting PSD can be seen in Fig. 4(a), whereas Fig. 4(b) shows the SER of the decoding scheme of Sec. III. There is a clear tradeoff in the selection of ϵ between OBR improvement and the required number of decoding iterations, a tradeoff which becomes more demanding for denser constellations. For instance, with $\epsilon = 0.015$, the proposed precoder achieves an
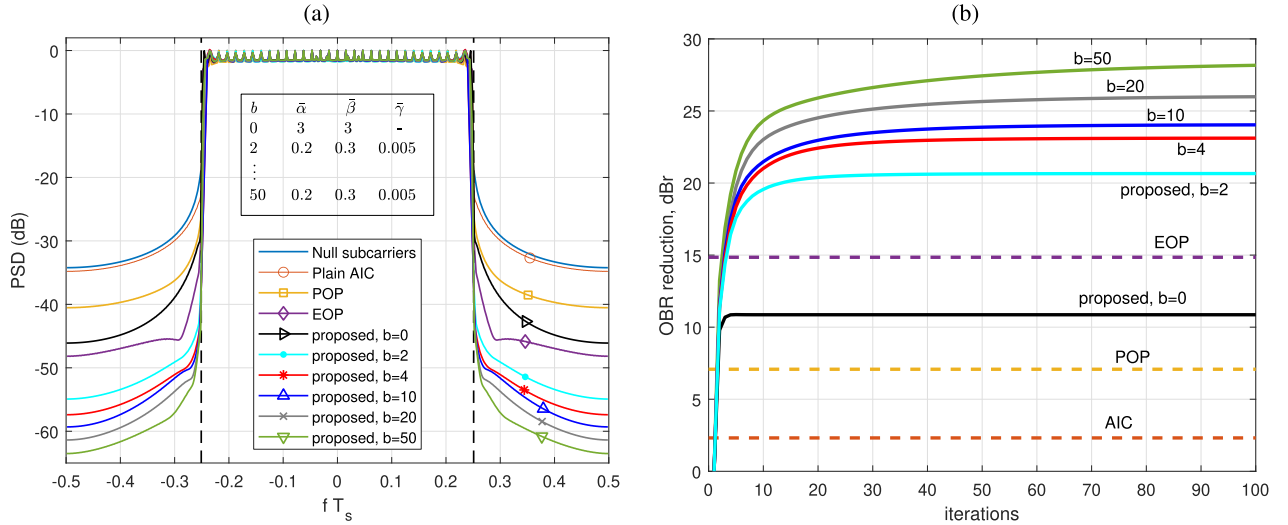
Fig. 3. Scenario 1: $K_c = 6$, $\epsilon = 0.005$. (a) PSD envelope; (b) Convergence of the proposed precoder design.
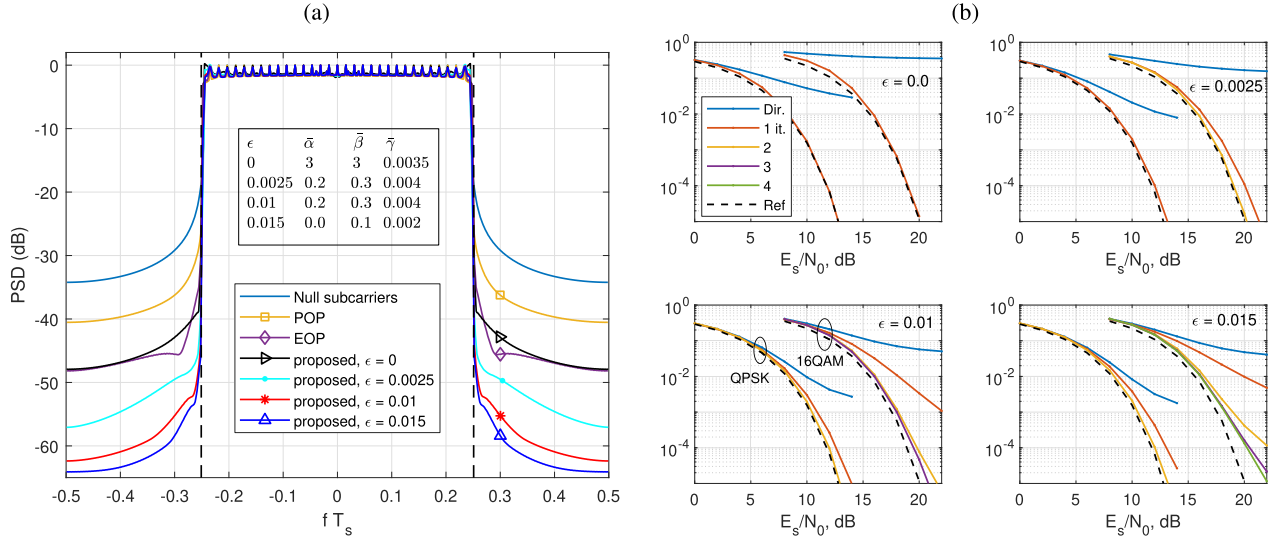

Fig. 4. Scenario 1: $K_c = 6$, $b = 10$. (a) PSD envelope; (b) Symbol error rate of the proposed decoding scheme with QPSK and 16-QAM in AWGN channel.

OBR reduction of 14.4 dB with respect to EOP; however, with 16-QAM the decoder takes about 3-4 iterations to converge, and it presents a 1-dB gap at SER$= 10^{-4}$ with respect to the baseline unprecoded system. Thus, for a given OBR level, the pair (b, ϵ) can be selected depending of the target SER and TX/RX complexities.

Fig. 5 shows the complementary cumulative distribution function (CCDF) of the Peak-to-Average Power Ratio (PAPR) of the multicarrier signals generated in this scenario. The PAPR degradation for the EOP scheme with respect to the unprecoded case with null subcarriers is 0.1 dB, and for the proposed scheme it remains within 1 dB. For fixed b the PAPR seems to be almost insensitive to the choice of ϵ, whereas for fixed ϵ PAPR degradation becomes worse for low values of $b > 0$. For $b = 0$ (not shown for clarity) the PAPR degradation of the proposed scheme is less than 0.1 dB.

Next, the number of cancellation subcarriers is reduced to $K_c = 2$ (redundancy $\frac{K_c}{K} = 0.8\%$). We fix $b = 10$, whereas now $\epsilon_k = \epsilon \in \{0, 0.005, 0.01, 0.015\}$, and $r_\Delta = 10$ is adopted for $\epsilon > 0$. The resulting PSD and SER curves are
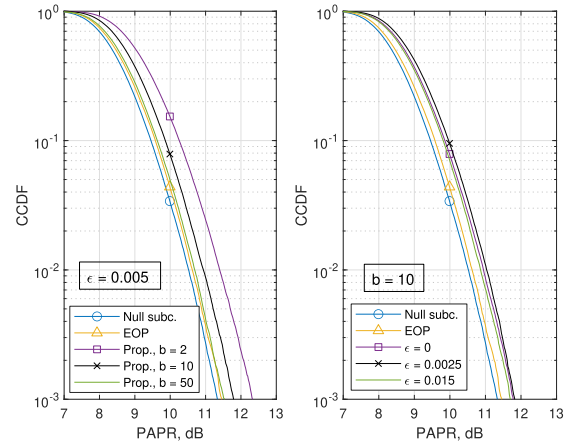

Fig. 5. Scenario 1: $K_c = 6$. PAPR with 16-QAM symbols.

shown in Fig. 6. In this low-redundancy setting, the orthogonal precoders cannot substantially improve performance with respect to simply turning off the cancellation subcarriers.
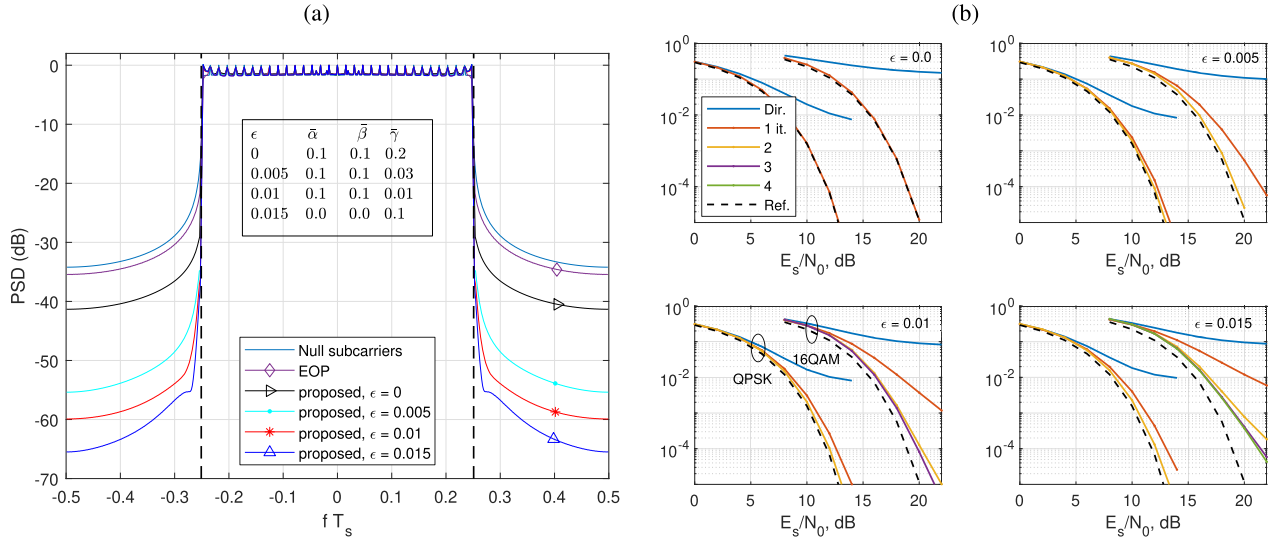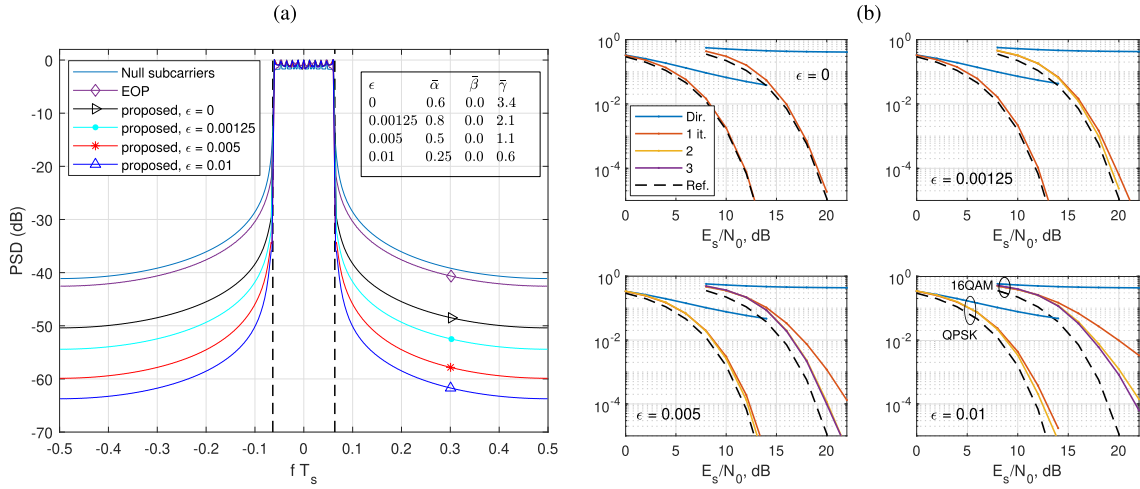
(a)   (b)

Fig. 6.   Scenario 1: $K_c = 2$, $b = 10$. (a) PSD envelope; (b) Symbol error rate of the proposed decoding scheme with QPSK and 16-QAM in AWGN channel.

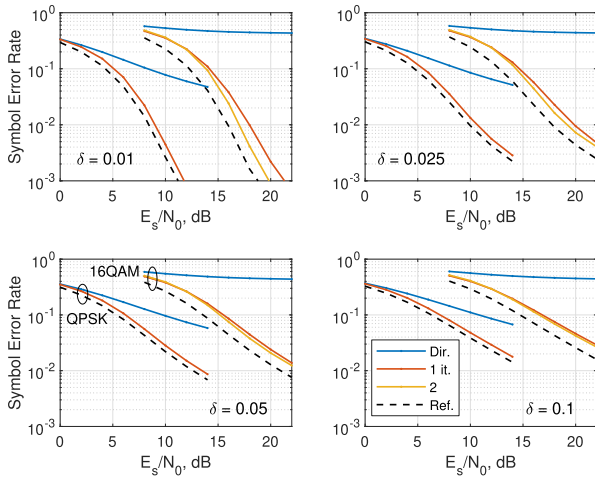(a)   (b)

Fig. 7.   Scenario 2: $K_c = 2$, $b = 4$. (a) PSD envelope; (b) Symbol error rate of the proposed decoding scheme with QPSK and 16-QAM in AWGN channel.

Fig. 8.   Scenario 2: $K_c = 2$, $\epsilon = 0.005$, $b = 4$. Symbol error rate of the proposed decoding scheme with QPSK and 16-QAM with a multipath channel.

The proposed scheme, in contrast, is able to reduce OBR significantly at the expense of increased complexity: for $\epsilon = 0$,

the number of cmults/symb at the TX and RX (with a single decoding iteration) is about twice that of EOP, whereas for $\epsilon > 0$ the corresponding complexities increase by factors of 4.4 at the TX and 5.4 at the RX (with two decoding iterations).

B. Scenario 2

In the second scenario, the number of active subcarriers is reduced to $K = 65$ with $\mathcal{K} = \{-32, \cdots, 0, \cdots, 32\}$. There are $K_p = 2$ protected subcarriers, with indices in $\mathcal{K}_p = \{\pm 9\}$, and $K_t = 9$ training subcarriers, with $\mathcal{K}_t = \{0, \pm 6, \pm 12, \pm 18, \pm 24\}$, so that $K_u = 54 - K_c$. The OBR region is now $\mathcal{B} = \{\frac{f_s}{16} + \frac{\Delta_f}{2} \leq |f| \leq \frac{f_s}{2}\}$, with weight function $W(f) = 1$ for $f \in \mathcal{B}$ and zero elsewhere. Only $K_c = 2$ cancellation subcarriers are available (redundancy $\frac{K_c}{K} = 3.1\%$), with indices in $\mathcal{K}_c = \{\pm 32\}$.

The resulting PSD and SER curves in AWGN channel obtained with $b = 4$ and for four different values of the normalized ICI power ϵ (with $\epsilon_k = \epsilon$ for all k) are shown in Fig. 7. Again, the reduced number of cancellation subcarriers
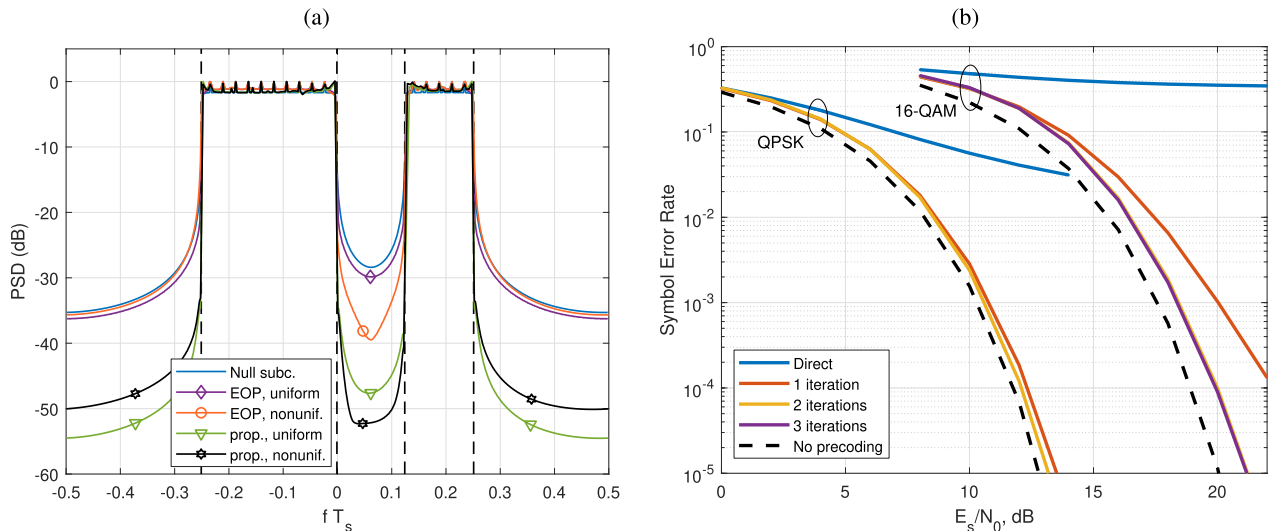
Fig. 9.   Scenario 3: $K_c = 4$, $b = 4$, $\epsilon = 0.005$. (a) PSD envelope; (b) Symbol error rate of the proposed decoding scheme with QPSK and 16-QAM in AWGN channel.

available results in poor performance of the orthogonal precoders, whereas the proposed design shows much better behavior. In all cases, a low-rank approximation of Δ with $r_\Delta = 8$ was adopted without noticeable degradation. Larger values of ϵ yield better OBR reduction, but with more decoding iterations needed at the receiver, and with an increasing gap with respect to the unprecoded reference system.

Next, we consider a multipath block-fading channel with exponential power delay profile. Specifically, channel taps are generated as $c[n] = e^{-\frac{n}{2\delta N_{cp}}} \cdot \tilde{c}[n]$, $0 \le n \le N_{cp}-1$, with $\tilde{c}[n]$ i.i.d. realizations of a circularly symmetric zero-mean complex Gaussian random variable. In this way, δN_{cp} corresponds to both the mean delay and the rms delay spread of the channel. The corresponding frequency-domain channel is normalized to yield $\sum_{k \in \mathcal{K}} |C[k]|^2 = K$. Fig. 8 shows the SER curves for the proposed decoder corresponding to a design with $\epsilon = 0.005$ and $b = 4$, assuming perfect channel knowledge and zero-forcing equalization; a different channel realization was independently drawn for each OFDM symbol. The proposed decoding scheme is seen to converge in a single iteration with QPSK with a gap smaller than 1 dB with respect to the baseline unprecoded system; with 16-QAM convergence is achieved in 1-2 iterations, and the gap is under 2 dB. SER performance is seen to degrade with increasing delay spread, as expected.

C. Scenario 3

Lastly, we consider a scenario with non-contiguous $K = 193$ active subcarriers, with indices in $\mathcal{K} = \{-1, -2, \cdots, -63\} \cup \{\pm 64, \pm 65, \cdots, \pm 128\}$. The protected subcarriers are at $\mathcal{K}_p = \{\pm 80, \pm 100\}$ ($K_p = 4$), and the training subcarriers are at $\mathcal{K}_t = \{\pm 72, \pm 84, \cdots, \pm 120\} \cup \{-12, -24, \cdots, -60\}$ ($K_t = 15$). Thus, in this case $K_u = 174 - K_c$. The OBR region is now $\mathcal{B} = \mathcal{B}_{out} \cup \mathcal{B}_{in}$, with

$$\mathcal{B}_{out} = \left\{ \frac{f_s}{4} + \frac{\Delta_f}{2} \le |f| \le \frac{f_s}{2} \right\},$$

$$\mathcal{B}_{in} = \left\{ -\frac{\Delta_f}{2} \le f \le \frac{f_s}{8} - \frac{\Delta_f}{2} \right\}.$$

The $K_c = 4$ cancellation subcarriers (redundancy $\frac{K_c}{K} = 2.1\%$) are placed at the spectrum edges: $\mathcal{K}_c = \{-128, -1, 64, 128\}$. We set $b = 4$ and $\epsilon_k = \epsilon = 0.005$ for all k, and consider two different spectral weighting functions:

- Uniform weight: $W(f) = 1$ for all $f \in \mathcal{B}$. Regularization factors $\bar{\alpha} = 0.1$, $\bar{\beta} = 0$, $\bar{\gamma} = 0.08$.
- Non-uniform weight: $W(f) = 1$ for $f \in \mathcal{B}_{out}$ and $W(f) = 10$ for $f \in \mathcal{B}_{in}$. In this way, more priority is given to low PSD levels over $\mathcal{B}_{in}$. Regularization factors $\bar{\alpha} = 10$, $\bar{\beta} = 0$, $\bar{\gamma} = 0.2$.

Results obtained with a low-rank approximation $r_\Delta = 10$ are shown in Fig. 9. The orthogonal precoder designed with a uniform weight yields little OBR reduction over either $\mathcal{B}_{out}$ or $\mathcal{B}_{in}$; with a nonuniform weight, the PSD over $\mathcal{B}_{in}$ is lowered by 10 dB. Nevertheless, the proposed design provides much better performance in this setting. It is seen that OBR reduction over $\mathcal{B}_{in}$ and $\mathcal{B}_{out}$ can be traded off by selecting the spectral weighting function. Regarding SER performance, the gap to the unprecoded reference system in AWGN channel is within 0.3 dB and 1 dB for QPSK and 16-QAM, respectively, with convergence taking place in two iterations in both cases.

VII. CONCLUSION

By allowing in-band distortion, the performance of spectral precoders can be significantly improved. Orthogonal precoders exploit this fact, providing satisfactory performance if sufficient redundancy can be afforded. However, in scenarios targeting high spectrum utilization, this may not be the case, and the proposed precoder design constitutes an alternative. The structure of the precoding matrix is selected with the operation of the decoder in mind, in order to allow compensation of in-band distortion. In this way, sidelobe reduction can be traded off against spectral redundancy, computational complexity, in-band spectral peaks, and error rate degradation, particularly with denser constellations.

The proposed decoding method targets low-complexity implementation and hinges on successive interference cancellation feeding back hard decisions on the data symbols, which

is not necessarily optimal. The development of alternative designs based on more sophisticated decoding schemes has the potential to reduce error rate degradation for spectral precoders aiming at aggressive sidelobe reduction, and constitutes an interesting line for future work.

APPENDIX A
SOLUTION TO (43)-(44)

In view of (6) and (7), one has $JC = J$ and $JCJ^H = I_{K_u}$. Using these, and introducing $B = \Pi^H S^H A_W S \Pi$ and $F = J\overline{G}_{j,k}^H A_W S \Pi$, the objective in (43) reads as

$$
\begin{aligned}
\operatorname{tr}\{G^H A_W G C\} = {} &\operatorname{tr}\{\overline{G}_{j,k}^H A_W \overline{G}_{j,k} C\} \\
&+ \operatorname{tr}\{\delta_k e_k^H B e_k \delta_k^H\} \\
&+ 2 \operatorname{Re} \operatorname{tr}\{F e_k \delta_k^H\}.
\end{aligned} \tag{52}
$$

$\overline{G}_{j,k}$ does not depend on δ_k, so (43)-(44) can be rewritten as

$$
\min_{\delta_k} (e_k^H B e_k)(\delta_k^H \delta_k) + 2\operatorname{Re}\{\delta_k^H F e_k\} \quad \text{s. to} \quad \delta_k^H \delta_k \le \epsilon_k. \tag{53}
$$

The unconstrained minimizer of the cost in (53) is given by $\delta_k = -\frac{F e_k}{e_k^H B e_k}$. If it is feasible, i.e., if $\frac{\|F e_k\|^2}{(e_k^H B e_k)^2} \le \epsilon_k$, then it also constitutes the solution to the constrained problem; otherwise, the constraint must hold with equality. The corresponding Lagrangian, with Lagrange multiplier λ, is

$$
\mathcal{L} = (e_k^H B e_k)(\delta_k^H \delta_k) + 2\operatorname{Re}\{\delta_k^H F e_k\} + \lambda(\delta_k^H \delta_k - \epsilon_k). \tag{54}
$$

Equating the gradient of $\mathcal{L}$ to zero yields $\delta_k = -\frac{F e_k}{e_k^H B e_k + \lambda}$. Substituting this in $\delta_k^H \delta_k = \epsilon_k$, one finds that $(e_k^H B e_k + \lambda)^2 = \frac{\|F e_k\|^2}{\epsilon_k}$; thus, $\delta_k = s\sqrt{\epsilon_k} \frac{F e_k}{\|F e_k\|}$, with $s \in \{-1, +1\}$. To remove the sign ambiguity, substitute this expression of δ_k in the objective of (53) to obtain

$$
\begin{aligned}
(e_k^H B e_k)&(\delta_k^H \delta_k) + 2\operatorname{Re}\{\delta_k^H F e_k\} \\
&= (e_k^H B e_k)\epsilon_k + 2s\sqrt{\epsilon_k}\|F e_k\|,
\end{aligned} \tag{55}
$$

which is minimized over $s \in \{-1, +1\}$ when $s = -1$. Thus, the solution to (53) can be compactly written as

$$
\delta_k = -\frac{1}{m} F e_k, \quad m = \max\{e_k^H B e_k,\ \|F e_k\|/\sqrt{\epsilon_k}\}. \tag{56}
$$

APPENDIX B
SOLUTION TO (45)-(46)

The component of G independent of Θ is given by

$$
\widetilde{G}_j = S\left[\Pi(I_{K_u} + \Delta_j)\ P_{\text{pt},j}\right] + T Q_j + R, \tag{57}
$$

so that $G = \widetilde{G}_j + S\Pi\Theta J$. Since $CJ^H = J^H$ and $JCJ^H = I_{K_u}$, one has

$$
\begin{aligned}
\operatorname{tr}\{G^H A_W G C\} = {} &\operatorname{tr}\{\widetilde{G}_j^H A_W \widetilde{G}_j C\} \\
&+ 2\operatorname{Re}\operatorname{tr}\{\Theta^H \Pi^H S^H A_W \widetilde{G}_j J^H\} \\
&+ \operatorname{tr}\{\Theta^H \Pi^H S^H A_W S\Pi\Theta\}. \tag{58}
\end{aligned}
$$

Let us write $\Theta = \begin{bmatrix}\theta_1 & \theta_2 & \cdots & \theta_{K_u}\end{bmatrix}$ columnwise. The constraint $\Theta \in \mathbb{L}_b^{K_u \times K_u}$ can be made explicit in terms of the columns $\{\theta_k\}$ as $\theta_k = E_k \widetilde{\theta}_k$, where for $k = 1, 2, \dots K_u - b$,

$$
E_k = \begin{bmatrix} 0_{k \times b} \\ I_b \\ 0_{(K_u - b - k) \times b} \end{bmatrix} \in \mathbb{C}^{K_u \times b}, \quad \widetilde{\theta}_k \in \mathbb{C}^b, \tag{59}
$$

whereas for $k = K_u - b + 1, \dots, K_u - 1$,

$$
E_k = \begin{bmatrix} 0_{k \times (K_u - k)} \\ I_{K_u - k} \end{bmatrix} \in \mathbb{C}^{K_u \times (K_u - k)}, \quad \widetilde{\theta}_k \in \mathbb{C}^{K_u - k}, \tag{60}
$$

and lastly $\theta_{K_u} = 0$. Thus, $\widetilde{\theta}_k$ comprises the nonzero elements of θ_k, and one can write $\Theta = \sum_{k=1}^{K_u} \theta_k e_k^H = \sum_{k=1}^{K_u - 1} E_k \widetilde{\theta}_k e_k^H$. Note that $\operatorname{tr}\{\Theta^H B\} = \sum_{k=1}^{K_u - 1} \widetilde{\theta}_k^H E_k^H B e_k$ for any $B \in \mathbb{C}^{K_u \times K_u}$. For ease of notation, let us introduce

$$
M_k = E_k^H \Pi^H S^H A_W S \Pi E_k \in \mathbb{C}^{n_k \times n_k}, \tag{61}
$$

$$
v_{j,k} = E_k^H \Pi^H S^H A_W \widetilde{G}_j J^H e_k \in \mathbb{C}^{n_k}, \tag{62}
$$

where $n_k = b$ for $1 \le k \le K_u - b$, $n_k = K_u - k$ for $K_u - b + 1 \le k \le K_u - 1$ is the number of columns of E_k. Then we can rewrite problem (45)-(46) as

$$
\min_{\{\widetilde{\theta}_k\}} \sum_{k=1}^{K_u - 1} \widetilde{\theta}_k^H M_k \widetilde{\theta}_k + 2\operatorname{Re} \sum_{k=1}^{K_u - 1} \widetilde{\theta}_k^H v_{j,k} + \gamma \sum_{k=1}^{K_u - 1} \widetilde{\theta}_k^H \widetilde{\theta}_k, \tag{63}
$$

which is convex quadratic. Its solution is given by

$$
\widetilde{\theta}_k = -(M_k + \gamma I_{n_k})^{-1} v_{j,k}, \quad k = 1, \dots, K_u - 1. \tag{64}
$$

APPENDIX C
ORTHOGONAL PRECODER DESIGN

Let R and Z be as in (4) and (39) respectively. Consider a precoder $G = ZF + R$, where $F \in \mathbb{C}^{(K_u + K_c) \times (K_u + K_p + K_t)}$ is to be optimized. This structure does not distort the protected and pilot subcarriers: with $x = Gd$, one has $R_p^H x = d_p$, $R_t^H x = d_t$. Let us partition $F = \begin{bmatrix} F_u & F_p & F_t \end{bmatrix}$, where $F_u \in \mathbb{C}^{(K_u + K_c) \times K_u}$, $F_p \in \mathbb{C}^{(K_u + K_c) \times K_p}$ and $F_t \in \mathbb{C}^{(K_u + K_c) \times K_t}$.

A. Plain Orthogonal Precoder

In this design we fix $F_p = 0$ and $F_t = 0$. Then, at the output of the receiver's zero-forcing equalizer, the vector of $K_u + K_c$ samples at unprotected and cancellation subcarriers satisfies $r_{uc} = F_u d_u + w_{uc}$, with w_{uc} the noise term. Thus, if F_u has orthonormal columns, $F_u^H r_{uc} = d_u + F_u^H w_{uc}$ approximately recovers d_u. The weighted power in (13) becomes $\mathcal{P}_W = \operatorname{tr}\{G^H A_W G C\} = \operatorname{tr}\{F_u^H Z^H A_W Z F_u\} + \operatorname{tr}\{R_{\text{pt}}^H A_W R_{\text{pt}} C_{\text{pt}}\}$, which is minimized over the set of semiunitary matrices when F_u comprises the K_u least eigenvectors of $Z^H A_W Z$. Since F_u has orthonormal columns, the products $F_u d_u$ (at the transmitter) and $F_u^H r_{uc}$ (at the receiver) can be efficiently performed by resorting to Householder reflectors [41], taking $2K_u K_c + K_c^2$ complex multiplications each.

B. Extended Orthogonal Precoder

Allowing $\boldsymbol{F}_\text{p}$, $\boldsymbol{F}_\text{t}$ to be nonzero, one has $\boldsymbol{r}_\text{uc} = \boldsymbol{F}_\text{u}\boldsymbol{d}_\text{u} + \boldsymbol{F}_\text{p}\boldsymbol{d}_\text{p} + \boldsymbol{F}_\text{t}\boldsymbol{d}_\text{t} + \boldsymbol{w}_\text{uc}$. The term $\boldsymbol{F}_\text{t}\boldsymbol{d}_\text{t}$ is known to the receiver, whereas an estimate $\hat{\boldsymbol{d}}_\text{p}$ can be readily obtained as shown in Sec. III. Thus, if $\boldsymbol{F}_\text{u}$ is semiunitary, and assuming $\hat{\boldsymbol{d}}_\text{p} \approx \boldsymbol{d}_\text{p}$, the receiver computes $\boldsymbol{F}_\text{u}^H(\boldsymbol{r}_\text{uc} - \boldsymbol{F}_\text{p}\hat{\boldsymbol{d}}_\text{p} - \boldsymbol{F}_\text{t}\boldsymbol{d}_\text{t}) = \boldsymbol{d}_\text{u} + \boldsymbol{F}_\text{u}^H\boldsymbol{F}_\text{p}(\boldsymbol{d}_\text{p} - \hat{\boldsymbol{d}}_\text{p}) + \boldsymbol{F}_\text{u}^H\boldsymbol{w}_\text{uc} \approx \boldsymbol{d}_\text{u} + \boldsymbol{F}_\text{u}^H\boldsymbol{w}_\text{uc}$, and again $\boldsymbol{d}_\text{u}$ is approximately recovered.

Let $\boldsymbol{F}_\text{pt} = \begin{bmatrix} \boldsymbol{F}_\text{p} & \boldsymbol{F}_\text{t} \end{bmatrix}$. It can be readily checked that the weighted power in (13) becomes $\mathcal{P}_\text{W} = \text{tr}\{\boldsymbol{G}^H\boldsymbol{A}_\text{W}\boldsymbol{G}\boldsymbol{C}\} = \text{tr}\{\boldsymbol{F}_\text{u}^H\boldsymbol{Z}^H\boldsymbol{A}_\text{W}\boldsymbol{Z}\boldsymbol{F}_\text{u}\} + \text{tr}\{(\boldsymbol{Z}\boldsymbol{F}_\text{pt} + \boldsymbol{R}_\text{pt})^H\boldsymbol{A}_\text{W}(\boldsymbol{Z}\boldsymbol{F}_\text{pt} + \boldsymbol{R}_\text{pt})\boldsymbol{C}_\text{pt}\}$. To avoid spectral peaks due to the term $\boldsymbol{F}_\text{pt}$, we introduce a regularization term and then solve

$$\min_{\boldsymbol{F}_\text{u}, \boldsymbol{F}_\text{pt}} \quad \mathcal{P}_\text{W} + \alpha' \|\boldsymbol{F}_\text{pt}\boldsymbol{C}_\text{pt}^{1/2}\|_F^2 \qquad \text{s. to} \quad \boldsymbol{F}_\text{u}^H\boldsymbol{F}_\text{u} = \boldsymbol{I}_{K_\text{u}}. \tag{65}$$

The solution to (65) is such that $\boldsymbol{F}_\text{u}$ comprises the K_u least eigenvectors of $\boldsymbol{Z}^H\boldsymbol{A}_\text{W}\boldsymbol{Z}$ and $\boldsymbol{F}_\text{pt} = -(\boldsymbol{Z}^H\boldsymbol{A}_\text{W}\boldsymbol{Z} + \alpha'\boldsymbol{I}_{K_\text{u}+K_\text{c}})^{-1}\boldsymbol{Z}^H\boldsymbol{A}_\text{W}\boldsymbol{R}_\text{pt}$. In this case, exploiting again the properties of Householder reflectors [41], and the fact that the term $\boldsymbol{F}_\text{t}\boldsymbol{d}_\text{t}$ can be precomputed and stored, the precoding operation at the transmitter takes $K_\text{u}(2K_\text{c}+K_\text{p})+K_\text{c}(K_\text{c}+K_\text{p})$ complex multiplications per OFDM symbol, and the same amount at the receiver for decoding.

REFERENCES

[1] *TS38.211: NR; Physical Channels and Modulation (Release 15)*, 3GPP, document TS38.211, Mar. 2018.

[2] *802.11ax-2021–Specific Requirements Part 11: Wireless LAN Medium Access Control (MAC) and Physical Layer (PHY) Specifications Amendment 1: Enhancements for High-Efficiency WLAN*, Standard IEEE 802.11ax-2021, May 2021.

[3] M. Faulkner, "The effect of filtering on the performance of OFDM systems," *IEEE Trans. Veh. Technol.*, vol. 49, no. 5, pp. 1877–1884, Oct. 2000.

[4] X. Huang, J. A. Zhang, and Y. J. Guo, "Out-of-band emission reduction and a unified framework for precoded OFDM," *IEEE Commun. Mag.*, vol. 53, no. 6, pp. 151–159, Jun. 2015.

[5] R. Zayani, Y. Medjahdi, H. Shaiek, and D. Roviras, "WOLA-OFDM: A potential candidate for asynchronous 5G," in *Proc. IEEE Globecom Workshops (GC Wkshps)*, Dec. 2016, pp. 1–5.

[6] M.-F. Tang and B. Su, "Joint window and filter optimization for new waveforms in multicarrier systems," *EURASIP J. Adv. Signal Process.*, vol. 2018, no. 1, pp. 63–82, Oct. 2018.

[7] K. Hussain and R. López-Valcarce, "Optimal window design for W-OFDM," in *Proc. IEEE Int. Conf. Acoust., Speech Signal Process. (ICASSP)*, May 2020, pp. 5275–5289.

[8] I. Cosovic and V. Janardhanam, "Sidelobe suppression in OFDM systems," in *Multi-Carrier Spread-Spectrum*, K. Fazel and S. Kaiser, Eds. Dordrecht, The Netherlands: Springer Netherlands, 2006, pp. 473–482.

[9] I. Cosovic and T. Mazzoni, "Suppression of sidelobes in OFDM systems by multiple-choice sequences," *Eur. Trans. Telecommun.*, vol. 17, no. 6, pp. 623–630, Nov. 2006.

[10] S. Pagadarai, R. Rajbanshi, A. M. Wyglinski, and G. J. Minden, "Sidelobe suppression for OFDM-based cognitive radios using constellation expansion," in *Proc. IEEE Wireless Commun. Netw. Conf.*, Oct. 2008, pp. 888–893.

[11] I. Cosovic, S. Brandes, and M. Schnell, "Subcarrier weighting: A method for sidelobe suppression in OFDM systems," *IEEE Commun. Lett.*, vol. 10, no. 6, pp. 444–446, Jun. 2006.

[12] R. Kumar and A. Tyagi, "Extended subcarrier weighting for sidelobe suppression in OFDM based cognitive radio," *Wireless Pers. Commun.*, vol. 87, no. 3, pp. 779–796, Apr. 2016, doi: 10.1007/S11277-015-2623-8.

[13] M. M. Naghsh, E. H. M. Alian, S. Khobahi, and O. Rezaei, "A majorization–minimization approach for reducing out-of-band radiations in OFDM systems," *IEEE Commun. Lett.*, vol. 21, no. 8, pp. 1739–1742, Aug. 2017.

[14] C.-D. Chung, "Spectrally precoded OFDM," *IEEE Trans. Commun.*, vol. 54, no. 12, pp. 2173–2185, Dec. 2006.

[15] J. van de Beek and F. Berggren, "N-continuous OFDM," *IEEE Commun. Lett.*, vol. 13, no. 1, pp. 1–3, Jan. 2009.

[16] J. Van De Beek, "Sculpting the multicarrier spectrum: A novel projection precoder," *IEEE Commun. Lett.*, vol. 13, no. 12, pp. 881–883, Dec. 2009.

[17] J. A. Zhang, X. Huang, A. Cantoni, and Y. J. Guo, "Sidelobe suppression with orthogonal projection for multicarrier systems," *IEEE Trans. Commun.*, vol. 60, no. 2, pp. 589–599, Feb. 2012.

[18] M. Mohamad, R. Nilsson, and J. van de Beek, "Minimum-EVM N-continuous OFDM," in *Proc. IEEE Int. Conf. Commun. (ICC)*, May 2016, pp. 1–5.

[19] K. Hussain, A. Lojo, and R. López-Valcarce, "Flexible spectral precoding for sidelobe suppression in OFDM systems," in *Proc. IEEE Int. Conf. Acoust., Speech Signal Process. (ICASSP)*, May 2019, pp. 4789–4793.

[20] K. Hussain and R. López-Valcarce, "OFDM spectral precoding with per-subcarrier distortion constraints," in *Proc. 27th Eur. Signal Process. Conf. (EUSIPCO)*, Sep. 2019, pp. 1–5.

[21] S. Kant, G. Fodor, M. Bengtsson, B. Göransson, and C. Fischione, "Low-complexity OFDM spectral precoding," in *Proc. IEEE 20th Int. Workshop Signal Process. Adv. Wireless Commun. (SPAWC)*, Jul. 2019, pp. 1–5.

[22] S. Kant, M. Bengtsson, G. Fodor, B. Göransson, and C. Fischione, "EVM-constrained and mask-compliant MIMO-OFDM spectral precoding," *IEEE Trans. Wireless Commun.*, vol. 20, no. 1, pp. 590–606, Jan. 2021.

[23] H. Yamaguchi, "Active interference cancellation technique for MB-OFDM cognitive radio," in *Proc. 34th Eur. Microw. Conf.*, vol. 2, 2004, pp. 1105–1108.

[24] S. Brandes, I. Cosovic, and M. Schnell, "Reduction of out-of-band radiation in OFDM systems by insertion of cancellation carriers," *IEEE Commun. Lett.*, vol. 10, no. 6, pp. 420–422, Jun. 2006.

[25] S.-G. Huang and C.-H. Hwang, "Improvement of active interference cancellation: Avoidance technique for OFDM cognitive radio," *IEEE Trans. Wireless Commun.*, vol. 8, no. 12, pp. 5928–5937, Dec. 2009.

[26] D. Qu, Z. Wang, and T. Jiang, "Extended active interference cancellation for sidelobe suppression in cognitive radio OFDM systems with cyclic prefix," *IEEE Trans. Veh. Technol.*, vol. 59, no. 4, pp. 1689–1695, May 2010.

[27] J. F. Schmidt, S. Costas-Sanz, and R. López-Valcarce, "Choose your subcarriers wisely: Active interference cancellation for cognitive OFDM," *IEEE J. Emerg. Sel. Topics Circuits Syst.*, vol. 3, no. 4, pp. 615–625, Dec. 2013.

[28] J. F. Schmidt, D. Romero, and R. López-Valcarce, "Active interference cancellation for OFDM spectrum sculpting: Linear processing is optimal," *IEEE Commun. Lett.*, vol. 18, no. 9, pp. 1543–1546, Sep. 2014.

[29] L. Díez, J. A. Cortés, F. J. Cañete, E. Martos-Naya, and S. Iranzo, "A generalized spectral shaping method for OFDM signals," *IEEE Trans. Commun.*, vol. 67, no. 5, pp. 3540–3551, May 2019.

[30] W.-C. Chen, C.-D. Chung, and P.-H. Wang, "Pre-equalized and spectrally precoded OFDM," *IEEE Trans. Veh. Technol.*, vol. 71, no. 7, pp. 7472–7486, Jul. 2022.

[31] R. Xu and M. Chen, "A precoding scheme for DFT-based OFDM to suppress sidelobes," *IEEE Commun. Lett.*, vol. 13, no. 10, pp. 776–778, Oct. 2009.

[32] J. van de Beek, "Orthogonal multiplexing in a subspace of frequency well-localized signals," *IEEE Commun. Lett.*, vol. 14, no. 10, pp. 882–884, Oct. 2010.

[33] M. Ma, X. Huang, B. Jiao, and Y. J. Guo, "Optimal orthogonal precoding for power leakage suppression in DFT-based systems," *IEEE Trans. Commun.*, vol. 59, no. 3, pp. 844–853, Mar. 2011.

[34] R. Kumar, K. Hussain, and R. López-Valcarce, "Mask-compliant orthogonal precoding for spectrally efficient OFDM," *IEEE Trans. Commun.*, vol. 69, no. 3, pp. 1990–2001, Mar. 2021.

[35] J. van de Beek, "OFDM spectral precoding with protected subcarriers," *IEEE Commun. Lett.*, vol. 17, no. 12, pp. 2209–2212, Dec. 2013.

[36] W.-C. Chen, J.-L. Jiang, and C.-D. Chung, "Cancellation symbol insertion technique for sidelobe suppression in OFDM pilot waveform," in *Proc. IEEE/CIC Int. Conf. Commun. China (ICCC)*, Aug. 2019, pp. 602–606.

[37] R. López-Valcarce, "General form of the power spectral density of multicarrier signals," *IEEE Commun. Lett.*, vol. 26, no. 8, pp. 1755–1759, Aug. 2022.

[38] G. H. Golub and C. F. Van Loan, *Matrix Computations*, 3rd ed. Baltimore, MD, USA: Johns Hopkins Univ. Press, 1996.

[39] J. F. Schmidt and R. López-Valcarce, "OFDM spectrum sculpting with active interference cancellation: Keeping spectral spurs at bay," in *Proc. IEEE Int. Conf. Acoust., Speech Signal Process. (ICASSP)*, May 2014, pp. 8053–8057.

[40] C. Eckart and G. Young, "The approximation of one matrix by another of lower rank," *Psychometrika*, vol. 1, no. 3, pp. 211–218, Sep. 1936.

[41] I. V. L. Clarkson, "Orthogonal precoding for sidelobe suppression in DFT-based systems using block reflectors," in *Proc. IEEE Int. Conf. Acoust., Speech Signal Process. (ICASSP)*, Mar. 2017, pp. 3709–3713.

Francesc Rey (Member, IEEE) was born in Barcelona, Spain, in 1973. He received the M.Sc. and Ph.D. degrees in telecommunication engineering from the Technical University of Catalonia (UPC), Barcelona, in 1997 and 2006, respectively. In 1998, he joined the Department of Signal Theory and Communications, UPC, where he has been an Associate Professor since April 2001. From 1998 to 2001, he held a grant from Generalitat de Catalunya in support of the Ph.D. degree. His current research interests include signal processing and communications, wireless MIMO channels, and distributed signal processing. He has been involved in many research projects in the framework of the research programs of the European Union, the European Space Agency, and Industry.

Khawar Hussain (Member, IEEE) received the B.Eng. degree in electrical engineering from the National University of Science and Technology (NUST), Islamabad, Pakistan, in 2012, the M.Eng. degree from the NED University of Engineering & Technology, Karachi, Pakistan, in 2016, and the Ph.D. degree from the University of Vigo, Vigo, Spain, in 2023. His research interests include signal processing and digital communications.

Josep Sala-Alvarez (Senior Member, IEEE) was born in Barcelona, Spain, in 1967. He received the M.Sc. and Ph.D. degrees in telecommunication engineering from the Technical University of Catalonia (UPC), Barcelona, in 1991 and 1995, respectively. In 1992, he was with the European Space Operations Centre (ESOC) of the European Space Agency (ESA), Darmstadt, Germany, in the area of software engineering for telemetry processing. From 1993 to 1994, he held a Grant from Generalitat de Catalunya in support of the Ph.D. degree with the Department of Signal Theory and Communications, UPC. In 1994, he joined UPC as an Assistant Professor and was promoted to an Associate Professor in 1997. He has participated in 13 space-related communication projects for ESA and in over 20 other wireless communications projects with industry and institutions at the national/European level, having been principal investigator in five research projects and in one research and development project. His long-standing research interests have been centered on signal processing for communications, in which area he has coauthored 20 journal articles, 55 international plus nine national conference publications, and having been advisor of four doctoral theses. Recently his research has focused on successive interference cancellation for massive random access. He was a recipient of the 2003 Best (Senior) Paper Award from the IEEE Signal Processing Society, the International Symposium on Turbo-Codes and Applications (ISTC '03) Best Poster Paper Award, and the Best Ph.D. Thesis in Telecommunication National Award, Spain, in 1995.

Roberto López-Valcarce (Senior Member, IEEE) received the degree in telecommunication engineering from the University of Vigo, Vigo, Spain, in 1995, and the M.S. and Ph.D. degrees in electrical engineering from the University of Iowa, Iowa City, IA, USA, in 1998 and 2000, respectively. In 1995, he was a Project Engineer with Intelsis. From 2001 to 2006, he was a Ramon y Cajal Post-Doctoral Fellow of the Spanish Ministry of Science and Technology with the Signal Theory and Communications Department, University of Vigo, where he is currently an Associate Professor. From 2010 to 2013, he was the Program Manager of the Galician Regional Research Program on Information and Communication Technologies. He has coauthored over 70 articles in leading international journals and is co-inventor in several patents in collaboration with industry. His main research interests include digital communications, adaptive and statistical signal processing, and sensor networks.

He was a recipient of the 2005 Best Paper Award from the IEEE Signal Processing Society. He was an Associate Editor of IEEE TRANSACTIONS ON SIGNAL PROCESSING from 2008 to 2011 and a member of the IEEE Signal Processing for Communications and Networking Technical Committee from 2011 to 2013. Since 2018, he serves as a Subject Editor for the *Signal Processing* journal.

Javier Villares (Senior Member, IEEE) was born in Barcelona, Spain, in 1974. He received the M.S. and Ph.D. degrees in telecommunication engineering from the Technical University of Catalonia (UPC), Barcelona, in 1999 and 2005, respectively. He has been an Associate Professor with the Department of Signal Theory and Communications, UPC, since 2003. His general research interests are digital communications, statistical signal processing, and information theory. He has combined fundamental research with the participation in numerous research projects in the area of wireless and satellite communications funded by the European Space Agency (ESA), the European Union, Industry, and the Spanish and Catalan research agencies.